
# Formulation of Lipid Nanoparticles with RNA-based Payload – Key Considerations for Characterisation

University of Nottingham

MRes Biomolecular Technology

Joseph Turpin

June 2025

Supervisors:

Professor Stephen Harding – University of Nottingham

Dr. Shahwar Jiwani – Sartorius Albumedix

# Table of Contents

# Abstract

Lipid nanoparticles are latest lipid-based drug delivery systems that have recently drawn attention for their use in vaccine preparations by moderna and Pfizer-BioNTech for the transport of mRNA during COVID-19 pandemic. LNPs allow for the transport of delicate drug payloads, which degrade or incite immunogenic responses during circulation at normal physiological levels. This literature review aims to identify possible techniques for preparation and characterisation of LNPs carrying RNA based payload.

The most common types of LNPs for RNA based cargo are solid lipid nanoparticles (SLNs) and nanostructured lipid carriers (NLCs). Both are suitable for transport. SLNs can carry both hydrophilic and hydrophobic drugs. NLC in comparison have greater biocompatibility due to a flexible membrane formed through structural tuning of surfactants used.

Surfactants such as ionisable lipids, PEGylated lipids, phospholipids and cholesterol have a key role in the structural characteristics and biocompatibility of the resultant LNPs. The combination of these components can be done in a variety of microfluidic mixers such as staggered Herringbone microfluidic mixer, an example of passive mixers. Chaotic flow in these passive mixers and increased surface area allows easy diffusion and mixing of aqueous and organic phase. Production of LNPs with passive mixers is preferred when handling RNA based cargo, to prevent the degradation of cargo through external interactions. Stability of LNPs can be measured by light scattering to identify PDI and zeta potential and aggregation behaviour. These parameters are important to predict the application in drug delivery.

This review focuses on the recent development in LNP based research and production. It aims to provide a comprehensive overview of different LNP formulations and their characterisation methods.

# 1. Introduction

Lipid nanoparticles (LNPs) are lipid-based structures, measured approximately 1000nm or smaller. They can be produced naturally during degradation of biological materials or found on the surface of plants. Recently LNPs have been used as a drug delivery vehicle. Such lipid-based encapsulation method was used for drug agent transport e.g. mRNA used in the COVID-19 vaccine and cancer immunotherapy as well as in gene editing (Mehta et al., 2023). Methods used to prepare RNA based vaccines such as those used during the coronavirus epidemic, have become an important alternative for vaccination development methods alongside conventional approaches. Inactive viruses have been regularly used to induce immunity through safe exposure of viral pathogens. Alternatively, mRNA vaccines, in which LNPs play an integral part of delivery, are based on the intracellular production of viral epitope proteins. As seen with the production of the COVID-19, preexisting knowledge of coronavirus structural proteins and epitopes allowed for a faster more efficiently produced vaccine. The use of mRNA-LNPs in the COVID-19 vaccine resulted in a faster more effective route of immunity compared to traditional viral vectors

LNPs allow for greater bioavailability and endosomal escape, increasing control of delivery targets and the regulation of the drug release (Mehta et al., 2023). Transport of delicate mRNA molecules within a lipid matrix circumvents rapid *in vivo* degradation experience because of blood serum temperatures, pH and the targeting of the reticuloendothelial system (RES). Reduced *in vivo* degradation results in an increase in serum half-life of the drug agent. Production of mRNA carrying LNPs requires the use of a variety of structural lipids present within the

lipid matrix. Cholesterol, ionizable, PEGylated, and phospholipids are important in determining the physiochemical properties expressed.

Formulation of LNPs have already been exhibited on large scales, seen during the production of COVID mRNA vaccines by Moderna and Pfizer-BioNTech. Production of LNPs can vary greatly due to mixing methods, components used and the methods in which physical and chemical properties of nanoparticles are recorded. This review identifies key structural components and their importance within the lipid matrix structure together with their influence on mRNA-LNPS. This study aims to use this information to determine suitable formulation parameters for the preparation of stable LNPs with the ability to encapsulate the payload at uniform size

## 1.1. Nanostructured lipid carriers and Solid lipid nanoparticles

Non-dissolving lipid carriers, solid lipid nanoparticles (SLNs), are capable of encapsulating both lipophilic and hydrophilic drugs. SLNs were first formulated in the early 1990s as an alternative solution to nano- and micro-drug carriers at the time such as liposomes and emulsions (Musielak, Feliczak-Guzik and Nowak, 2022). Unlike liposomes which have limited possibility for modifications within the surface structure, or foundational lipids due to the ordered conformation of the lipid bilayer, SLNs have an amorphous membrane structure formed from a single layer of highly purified triglycerides. This allows for the addition of structurally reenforcing surfactants such as polyethylene glycols (PEG), cholesterol, phospholipids and ionized lipids increasing molecular stability and the serum half-life thereby allowing for more effective transport of therapeutic agents while being physically stable at room temperature (Chauhan et al., 2020).

SLNs are formulated from solid lipids, for example such as fatty acids, triglycerides, steroids, glycerides and stearic acids. These biocompatible structural molecules are tolerable for the human body, resulting in minimal toxicity during transport. Literature describes SLNs as mostly spherical in shape with a diameter between 10 and 1000nm and stable under normal physiological body temperatures (Musielak, Feliczak-Guzik and Nowak, 2022). SLNs can control the rate of drug release through hinderance of the agent's diffusion via the lipid scaffold, providing sustained release and the reduction in toxic side effects.

Due to their flexible membrane composition in comparison to SLNs, the membranes of nanostructured lipid carriers (NLCs) can be tuned via the mixing ratios of solid and liquid lipids during formulation. Structural tuning allows for changes in the lipid nanoparticles therapeutic release profile to be altered enabling tailoring to temperature and pH profiles of patients or agents used (Marjorie and Luís Alexandre Muehlmann, 2024). Figure 1 highlights the structure in which components such as lipids and surfactants are used. The characteristic expressed in LNPs is dependent on the constituents and the formulation method used during production. Long chained triglycerides are the most commonly used lipids when formulating lipid nanoparticles due to their high melting point and physical stability which promotes long term release of the therapeutic agent, further improving the drugs bioavailability and extending the effective therapeutic time before another dose is required. Liquid lipids such as medium-chain triglycerides and unsaturated oils are required to produce a flexible and fluid matrix. Liquid at room temperature and in serum, liquid lipids prevent excess rigidity of the molecule resulting in increased load capacity and cellular uptake. The presence of both solid and liquid lipids forms a stable particle which has a high bioavailability.

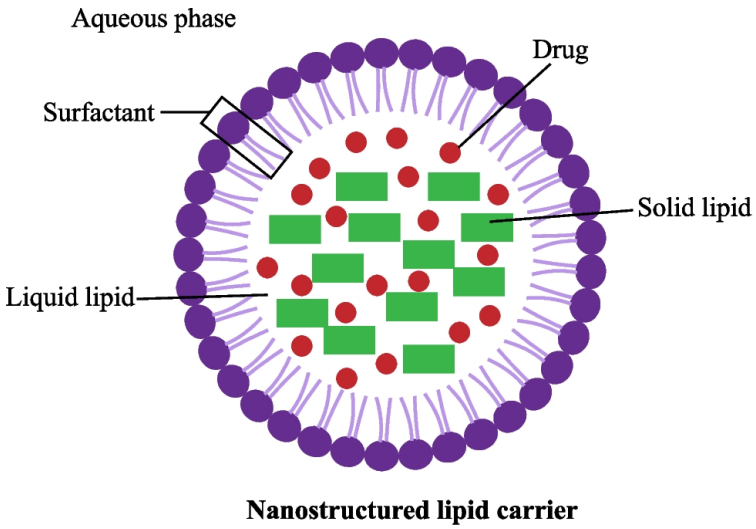


**Figure 1***:* A diagram (Soni, Maheshwari and Sah, 2024) showcasing the constitution of Nanostructured lipid carriers (NLCs). The drug is suspended in a mixture of solid and liquid lipids surrounded by a lipid matrix consisting of numerous surfactants; including ionizable, PEGylated and phosphorylated lipids as well as cholesterol which aid in the stability and flexibility of the NLC. In contrast SLNs present the same lipid matric with the therapeutic agent contained within solid lipids only.

## 1.2. Structural surfactants

LNP physical and chemical properties are determined by the structural surfactants used. Outside of the core structure of the lipid matrix, surfactants such as ionizable lipids, PEGylated lipids, phospholipids and cholesterol alter the lipid matrix flexibility, extracellular structure and ability for cargo encapsulation.

Ionizable lipids, used for the encapsulation and transportation of mRNA, are an important tool for *in vivo* delivery of bioactive materials. Ionizable lipids are pH responsive, stable at physiological pH levels of 7.4 which allows for stable LNP function throughout circulation (Wang et al., 2024). The ability to change the charge depends on environmental pH that prevents unwanted interactions with anionic compounds other than mRNA such as immune cells. Under acidic conditions as seen during the presence of endosomes where the pH ranges between 5.5 and 6.3, ionizable lipids become positively charged. Positively

charged ionizable lipids facilitate endosomal escape through interactions through pronation and subsequent interactions with negatively charged phospholipids (Wang et al., 2024). Protons are accumulated by the functional groups on ionizable lipids. An increase in positive charge within the endosome increases the fluid movement leading to a turgid state and eventual bursting of the endosomal membrane consequently releasing therapeutic cargo within the cytoplasm (Haque et al., 2024). The ability to induce protonation via ionizable lipids during the endosomal escape of LNPs increases the bioavailability through increased cytoplasmic transfer efficiency.

Polyethylene glycol (PEG) is a commonly used structural enhancer, conjugated to structural lipids to form PEGylated lipids. The addition of PEG chains imparts 'stealth' properties to LNPs. LNPs are viewed as foreign molecules and attacked by the reticuloendothelial system (RES) that is comprised of dendritic cells, blood monocytes and tissue-resident macrophages (Suk et al., 2016). The RES system identifies nanoparticles as pathogenic due to the absorption of opsonin's. Opsonin's stimulate immune-signalling molecules such as fibronectin and lipoproteins which bind to the matrix surface inciting immunogenic reactions from monocytes such as macrophages (Suk et al., 2016). Steric hinderance seen via PEGylation reduces binding of undesired signalling molecules preventing degradation because of RES. PEGylation of the LNPs matrix reinforces the structure from phagocytosis and aggregation through steric stabilization. The addition of flexible hydrophilic chains on the surface of the predominantly hydrophobic lipid matrix hinders self-aggregation and cellular fusion, resulting in increased bioavailability and serum half-life (Jung et al., 2022). Although PEGylation aids in the prevention of LNP aggregation, self-aggregation can occur when lipids are in aqueous conditions. Van der Waals forces induce self-assembly;

this effect is exacerbated in highly ionic environments such as blood serum resulting in the formation of electrostatic bonds. Prevention of large aggregate formation is essential to prevent the risk of capillary blockage in pulmonary tissue (Jung et al., 2022).

Phospholipids and cholesterol aid in a more general sense than PEGylation and ionizable lipids previously mentioned. Both phospholipids and cholesterol aid in structural support and the biodistribution of LNPs, increasing intracellular uptake through endosomal escape and cytoplasmic entry. One of the most used phospholipids is 1,2-distearyol-sn-glycero-3-phosphocholine (DSPC) used in siRNA therapy and mRNA vaccines' DSPC was one of the surfactants used in the SARS-CoV-2 (Jung et al., 2022). DSPC is a cylindrical saturated acyl group with one or more double bonds with a high melting point which provides a load bearing to the outer lipid matrix. In addition to increasing the stability and half-life of the nanoparticle, this also results in reduced endosomal escape as binding of the LNP to the inner endosome membrane is blocked. Another commonly used acyl-based phospholipid is 1,2-dioleoyl-sn-glycero-3-phosphoethanolamine (DOPE). DOPE has two acyl chains and a hydrocarbon chain (Jung et al., 2022). Unlike DSPC, DOPE has a low melting temperature and increasing endosomal escape capabilities.

Cholesterol is a regulator of membrane stability and rigidity, controlling the transfection of genetic material and release of the encapsulated drug. Modifications to cholesterol can improve the mRNA delivery. The addition of hydroxyl groups enhances the disruption of the endosomal membrane resulting in better endosomal escape of the mRNA agent (Wang et al., 2024). A reduction in nanoparticle size can be seen for lipid nanoparticles formed during an increase in

the molar ratio of cholesterol, indicating that cholesterol is a controlling factor on the size of the LNP (Jung et al., 2022).

## 1.3. LNP as mRNA delivery tool

LNPs are encapsulation and carrier molecules that have been critical in the formation of RNA based therapeutics. mRNA therapy is an efficient method for the treatment of infectious diseases, cancer and metabolic diseases; however, mRNA is naturally delicate and subject to degradation. *In vivo* delivery of mRNA can lead to RNase exposure and subsequent degradation aiding to poor bio-efficiency and lack of membrane penetration (Machado et al., 2021). Prevention of RNase degradation and increasing membrane penetration can be achieved using LNPs such as solid lipid nanocarriers and nanostructured lipid carriers (Machado et al., 2021). Bioavailability depends on particle size, charge and degradation, which all aid lipid encapsulation, inducing of endosomal escape and immune evasion of mRNA during systemic distribution. The bioavailability of mRNA therapeutic agents carried in LNPs can be further increased through the addition of surfactants.

Other delivery methods are capable of delivering RNA based therapeutics. Viral vectors have previously been used for mRNA delivery. Which, although effective, viruses such as adenovirus promote immunogenic reactions limiting their repeatable usage per patient (Haque et al., 2024). Another example is polymeric nanoparticles. Protection of RNA occurs through the biodegradable polymer membrane; however, endosomal escape is not as efficient as for LNPs (Haque et al., 2024). The lack of ionizable lipids with the ability for protonation and subsequent endosomal escape and cargo release, make them inefficient. In comparison LNPs evade the immune system allow for effective transfer of mRNA and have a much larger load capacity in comparison to other delivery mechanisms.

## 1.4. Methods for the preparation of LNP production

Microfluidic staggered Herringbone micromixers are one of the most commonly used microfluidic chips. These chips employed a passive mixing method that does not require energy input or active parts to complete mixing.

Microfluidic mixing is the use of small flow channel mixing to increase the surface to volume ratio of the mixed products and resulting in the self-assembly of small LNPs. Aqueous phase containing water or another miscible liquid together with the desired drug are fed into a central channel meeting the organic phase that contains structural lipids and other necessary surfactants (Suh and Kang, 2010). Although gaining greater control over the size of the LNP produced it is still difficult to tune completely, therefore LNPs are adjusted in 5-10nm intervals (Li, Miao and Tong, 2024). Microfluidic mixers, made from non-reactive materials such as glass or silicon cause aqueous and organic mixtures to encapsulate at a higher efficiency in comparison to other mixing methods such as emulsification, in addition to drug loading, leading to slower rates of release (Williams, Longmuir and Yager, 2008). Microfluidic mixing is often characterised by the Reynolds number ($Re = \rho UL/\mu$, where $\rho$ is liquid density), identifying the flow type within the channels, Reynolds numbers $<2000$ are commonly laminar flow, in which mixing is dependent on molecular diffusion and is insufficient for nanoparticle formation (Lee et al., 2011).

Multiple microfluidic mixing techniques are available including intersecting channel mixing and pulse flow mixing. Pulse flow mixing is an active mixing technique whereby mixtures are injected in an alternating pattern. This is a popular active mixing technique for increased mixing efficiency without the presence of complicated channel geometry as seen in passive mixers. Samples are injected through electroosmosis, moving sample liquids through the microchannels via

(Suh and Kang, 2010). Mobile ions within the electron double layer on the microchannel surface flow when an electric current is applied to the channel. This results in turbulent fluid flow in the material within the channels. Although allowing for precise mixing, this method only allows for mixing at the entrance to the channel and could be improved with the addition of geometric structures like those found in the staggered herringbone method (Suh and Kang, 2010). However, active mixing techniques use expensive machinery, and the use of electric fields can possibly damage the sample product. Passive mixers increase the contact area of fluids through structural design instead of active movement seen in pulse flow mixing.

Intersecting channel micromixers use a primary snaking channel with perforated walls which travel parallel to the main channel allowing for splitting and folding of mixtures (Lee et al., 2011). The stretching for the contacted area between the two sample liquids allows for more surface diffusion to occur increasing the speed of the mixing process. This occurs due to pressure from one mixed liquid pushing the other against the perforated wall, although not strong enough to break surface tensions and for the liquid through the perforation, enough liquid will be pushed through the perforation, wetting the wall of the channel downstream, increasing the contact area for mixing as the liquids pass by (Lee et al., 2011).

Initiation of LNP self-assembly is driven through a solvent based mixing method relying on rapid evaporation. Solvent emulsification involves two steps, the preparation of aqueous and organic phases. Therapeutic agents are added to the aqueous phase and mixed with the organic phase to form nano-emulsions (Marjorie and Luís Alexandre Muehlmann, 2024). Common solvents used include dichloromethane, chloroform and cyclohexane. Subsequently, mechanical stirring and warming, evaporates the solvents producing lipid droplets, which when

increased in concentration results in the formation of SLNs or NLCs due to lipid precipitation (Nguyen and Duong, 2022). Due to the use of toxic solvent compounds, LNPs formed using solvent-based methods require sufficient testing of the formulation *in vitro* and *in vivo* to ensure all toxic solvent compounds have been evaporated and removed (Nguyen and Duong, 2022). This method is suitable for drugs which are thermally unstable. However, herringbone formulation uses a slightly different preparation method. The aqueous and organic phases are prepared in a similar fashion to solvent emulsification; however, the aqueous phase is a solution with an emulsifier in the place of a solvent. The organic phase is then injected into the aqueous phase and mixed thoroughly in the herringbone mixer for the formation of lipid capsules.

Total Flow Rate (TFR) and Flow Rate Ratio (FRT) are important parameters in microfluidic LNP development. TFR is a ratio between the flow of the aqueous and organic phases during mixing. High TFRs cause increased advection during mixing forming a more chaotic flow and decreasing mixing times (Johnson, Ross and Locascio, 2002). Slow flow rates can result in in a more laminar flow potentially forming LNPs with high PDI and low encapsulation (Johnson, Ross and Locascio, 2002). The FRR defines the individual flow rates of the aqueous and organic phases. The greater the contrast in flow rates between phases produces LNPs with a smaller hydrodynamic diameter and a lower PDI due to rapid dilution of ethanol. Dilution of ethanol increases the solvent polarity causing rapid lipid self-assembly (Ripoll et al., 2022). Roces et al. (2020) compared differences in PDI and zeta potential of different TFR and FRR when formulating LNPs with MC3. They identified lower flow rates (5mL/ min) to have the highest PDI. Interestingly, after dialysis, the 10mL/ min and 20mL/ min, TFR showed little difference in PDI. Their comparison of FRR after dialysis highlighted the effectiveness of increasing solvent

polarity through ethanol dilution. The high FRRs (3:1 and 5:1) showed little difference in LNP parameters with PDI > 0.2 similar average hydrodynamic diameter. In contrast, an FRR of 1:1 had a significantly average diameter and high PDI with large standard deviations, indication poor uniformity.

Haque et al. (2024) describe LNP components to typically include ionisable lipids (30-50%), phospholipids (10-20%), PEGylated lipids (0.5-5%) and cholesterol (20-50%). The ratio in which these are mixed influence the hydrodynamic diameter, PDI, surface charge and encapsulation efficiency. The greatest fraction for RNA-based LNP production is the ionisable lipid, up to 50% of the total lipid components present. Ionisable lipids such as MC3 hold positively charge, driving the encapsulation of negatively charged mRNA. As previously stated, it also has a key role in the cellular uptake of the cargo, making it the most important factor in successful LNP encapsulation. The component mixing ratios are heavily dependent on the desired payload and the target destination (Ripoll et al., 2022). LNPs can be tailored for desired traits including stability and endosomal release of the payload via alterations of lipid constituents used and their relative proportions.

Table 1 shows the lipid components used, and the respective ratios used during LNP formulation with a focus on the D-Lin-MC3-DMA (MC3) ionisable lipid. Literature shown in table one have similar mixing ratios and components differing mostly with the used mixing chips, with Ignite nano-assembly and its predecessor *assembly* chips. Ignite assembly uses a ring like structure in comparison to its predecessor which utilises the staggered herringbone mixer. MC3 protocols commonly used a 3:1 ratio and a flow rate of 12mL/ min. Most formulations were tested for the PDI, Zeta potential using DLS and their encapsulation efficiency via a fluorescent dye assay. Notably Yavuz et al. (2023) and Anna Laura Nelson et al. (2024) had similar techniques but produced LNPs with the same parameters

but different sizes. The main difference being the mixing chip (nano-assembly and Ignite nano-assembly) and TFR (12mL/ min and 9mL/min). Yavuz et al. (2023) was able to produce LNPs with an average diameter between 75nm and 80nm, 30nm smaller than Anna Laura Nelson et al. (2024). Although both techniques produced LNPs with a low PDI, high zeta potential and an encapsulation efficiency above 90%, the difference in size of LNPs produced highlights in importance of TFR for the control of LNP hydrodynamic diameters.

***Table 1:*** Overview of mixing strategies used in published LNP formulations.

| Components organic phase | Mixing Ratio | Mixing chip | Total flow rate | Flow Rate Ratio | Testing methods used | Reference |
|---|---|---|---|---|---|---|
| DSPC: Chol: MC3: DMG-PEG2k | 10:37:50:3/ 10:38.5:50:1.5 | Ignite nanoassembly | 12mL/min | 3:9 | DLS - PDI/Z - potential, Ribogreen Assay | (Feng, 2024) |
| DSPC: Chol: MC3: DMG-PEG2k | 10: 48: 40: 2 | Y-shape staggered herringbone | 10mL/min | 3:1/ 5:1 | DLS - PDI/ Z - potential | (Roces et al., 2020) |
| DSPC: Chol: SM-102: DMG-PEG2k | 10:38.5:50:1.5 | Ignite Nanoassembly | 12ml/ min | 1:3 | DLS - PDI/ Z - potential | (Lee et al., 2024) |
| DSPC: Chol: MC3: DMG-PEG | 10:38.5:50:1.5 | T junction | Not stated | Not stated | DLS – PDI – Ribogreen assay | (Ferraresso et al., 2022) |
| DSPC: Chol: MC3: DMG-PEG2k | 10:48:40:2 | T-junction | Not stated | Not stated | DLS – PDI | (Geall et al., 2012) |
| DSPC: Chol: MC3: DMG-PEG2k | 10:38.5:50:1.5 | staggered Herringbone (nanoassembly) | 12mL/min | 3:1 | DLS - PDI/ Z - potential, Quant-iT - | (Binici et al., 2024) |
| DSPC: Chol: MC3: DMG-PEG2k | 10:38.5:50:1.5 | Staggered Herringbone | 12mL/min | 3:1 | DLS - PDI/ Z - potential, Quant-iT | (Jürgens et al., 2023) |
| DSPC: Chol: MC3: DMG-PEG2k | 10:38.5:50:1.5 | Ignite nanoassembly | 12mL/min | 3:1 | DLS - PDI/ Z - potential, Quant-iT ribgreen | (Yavuz et al., 2023) |
| DSPC: Chol: MC3: DMG-PEG2k | 10.5:38:50:1.5 | nanoassembly | 9ml/ min | 3:1 | DLS - PDI/Z - potential, Ribogreen | (Anna Laura Nelson et al., 2024) |

## 1.5. Microfluidics – the herring bone method

The staggered herringbone mixer is an example of microfluidic mixers which causes chaotic advection through geometric structures within the channel. Chevron grooves at the base of the channel, as seen in Figure 2, increases the entropy of the two distinct liquids for effective encapsulation to occur (Suh and Kang, 2010). The herringbone grooves in one or more of the walls of the micro-channel induce a transverse flow, resulting in two counter rotating vortices throughout the channel, reorienting at half-cycle intervals caused by the offset grooves of the herringbone, extending from the middle of the channel and producing a more effective and chaotic mixing environment (Suh and Kang, 2010).

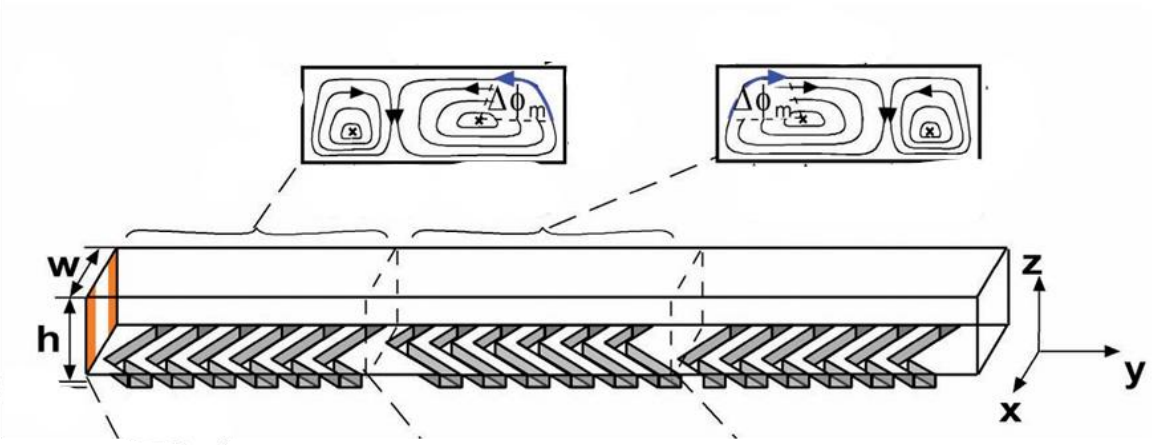


**Figure 2***:* A diagram (Stroock et al., 2002) identifying the mixing environment created through the addition of chevron grooves at the base of a herringbone mixing. Three half cycles are present in the diagram for each half cycle the direction of the grooves change and subsequently the direction of turbulence can be seen increasing the chaotic environment aiding to more through mixing.

Passive mixers produce chaotic mixing environments via geometric structures, such as the grooves within the SHM, and without active parts or external energy supply. When the Reynolds number (Re) is low (~1), passive mixers such as herringbone and serpentine mixers experience reduced mixing ability in relation to an increase in sample mass increase. This highlights the dominance of molecular diffusion in laminar flow in passive mixing instruments (Suh and Kang,

2010). In addition, increasing fluid viscosity through greater solute concentrations lowers the Reynolds number, further reducing the efficiency of mixing under laminar flow, resulting in a less homologous mixture. Although decreasing the mixing capabilities in serpentine mixers, herringbone mixers saw an increase in mixing efficiency, indicating flow convection aids and improvements on classic passive microfluidic structures (Suh and Kang, 2010).

## 1.6. Testing Methods

### 1.6.1. Dynamic light scattering – polydispersity testing

Dynamic light scattering (DLS) is widely used for LNP characterisation. DLS uses the principle of Brownian motion, measuring the light interference of LNPs in a suspension (Cho et al., 2013). Light scattering occurs when the light from a monochromatic laser interacts with nanoparticles in suspension, causing the light to be redirected in various directions due to differences in the refractive index between the tested nanoparticles and the surrounding medium (Stetefeld, McKenna and Patel, 2016). Brownian motion is the cause of light intensity fluctuations; random movement of the sample particles are a result of interactions with the suspension medium. Brownian motion is characterized as the diffusion coefficient. The size of the diffusion coefficient (*D)* depends on the size of the tested particle.

Characterisation of LNPs after formulation is essential to determining the particle size, polydispersity index (PDI), zeta potential (surface charge), encapsulation efficiency and molecular weight which allow for an understanding of the stability of the LNPs produced. These characteristics are important to understand how changes can affect production and ensure consistency between production batches (Mehta et al., 2023). The PDI is a measure of the size distribution between all

molecules produced, allowing estimations for the subsequent biodistribution and serum half-life of LNPs. As the LNPs move randomly throughout the solution they collide with the solvent molecules, a laser beam is shone through the solution scattering light at different intensities to surrounding detectors. Figure 3A shows a speckled pattern of light and dark patches. These patches are how the scattered light signals interact with each other during DLS resulting in light intensity patches. Where light patches are seen the scattered light has been enhanced. Enhancement occurs when scattered light signals have the same phase (Vasile-Dan Hodoroaba, Wolfgang E S Unger and Shard, 2020). Where light is traveling at synchronized wavelengths, a greater intensity can be detected. Dark patches are signifiers of destructive interference, unsynchronized waves arriving at the detector out of phase produce opposing signals (Vasile-Dan Hodoroaba, Wolfgang E S Unger and Shard, 2020). Figure 3B shows how these constructive and destructive signals affected the overall recorded light intensity over time. Large articles are seen to have a more steady, slower change in intensity in comparison to small particles. This is due to small particles having greater movement in suspension, forming a greater number of speckled patterns resulting in a greater number of changes in intensity (Bhattacharjee, 2016).

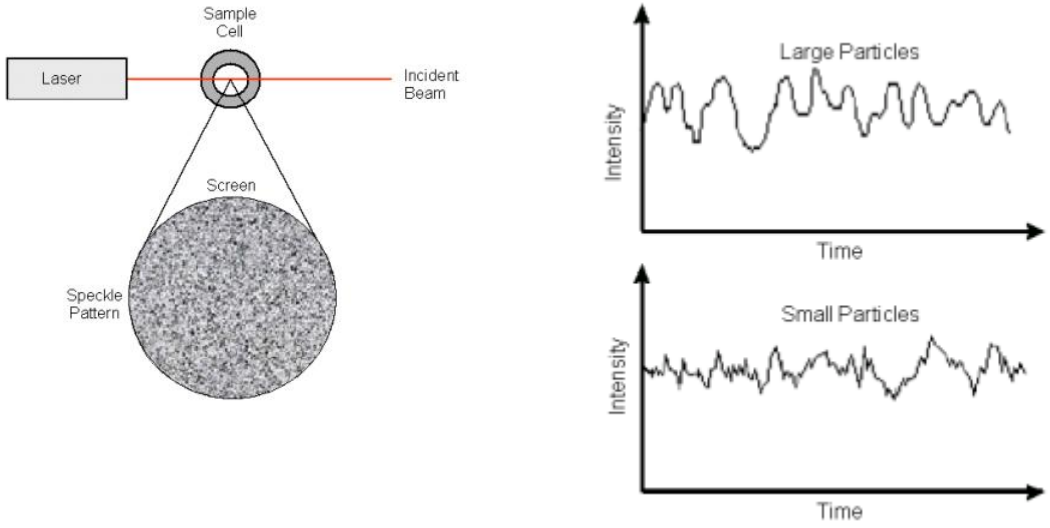


**A** **B**

**Figure 3A***: A* diagram showing the light scattering speckle pattern produced through enhanced and destructive waves lengths in which signal intensities are compared by the auto correlator to quantify the Brownian motion of the molecules in suspension, providing the diffusion coefficient (Malvern Instruments, 2017). **Figure 3B** shows two detected light intensity graphs of large and small molecules samples. The large molecules diffuse slower, resulting in more gradual changes in light intensity. In comparison, small molecules, with rapid random movement have much greater changes in detected light intensity, representative of their small size and rapid Brownian motion. (Malvern Instruments, 2017)

Polydispersity is measured on a scale between 0 and 1, with the completely homozygous populations being 0, a PDI < 0.3 is the highest acceptable limit of PDI for a product to be labelled as a homogenous population (Mehta et al., 2023). The intensities of the scattered light are compared against the diffusion coefficient of the predicted molecule using the Strokes-Eistein equation (1) to produce the hydrodynamic diameter and subsequently the poly dispersity index (Stetefeld, McKenna and Patel, 2016). The diffusion coefficient is calculated through the autocorrelator function. It measures the degree of similarity between two signals or one signal with itself at differing timepoints. As time progresses the signal correlation will at some point bear no similarity to the original signal for truly random movement of particles. The diffusion coefficient is calculated from the time taken for the signal to have no correlation, in turn allowing the size of the particle

to be calculated from the distribution of the hydrodynamic diameter a sample's (Stetefeld, McKenna and Patel, 2016).

$$d(H) = \frac{kT}{3\pi\eta D} \quad (1)$$

In the Stokes-Einstein equation $d$(H) is the hydrodynamic radius, $k$ is the Boltzmann constant and $T$ the absolute temperature (K), η is the viscosity of the suspension and $D$ is the diffusion coefficient (Vasile-Dan Hodoroaba, Wolfgang E S Unger and Shard, 2020). The hydrodynamic radius calculated is produced in relation to the Brownian motion of the particle throughout testing and can be affected by parameters such as ionic interactions with the medium and particle shape. The shape of nanoparticles and the membrane bound surface structures can reduced the speed of diffusion of particles throughout the medium.

### 1.6.2. Zeta Potential

The ionic charge of the suspension medium can influence the accuracy of the hydrodynamic diameter of LNPs. Zeta potential is the surface charge of a tested molecule giving an insight into the behaviour of the molecule and likelihood of aggregation within a suspension. Charged particles have a double electron layer, the net charge of the molecule attracts ions of opposing charge resulting in a surrounding layer of charged particles (Chakraborty and Panigrahi, 2020). These can be divided into two layers, as seen in figure 4, the inner stern which is strongly bound and the outer diffuse layer which is loosely related to the molecule and is responsible for the rate of movement and diffusion of the molecule. The charge of this outer layer is the zeta potential.

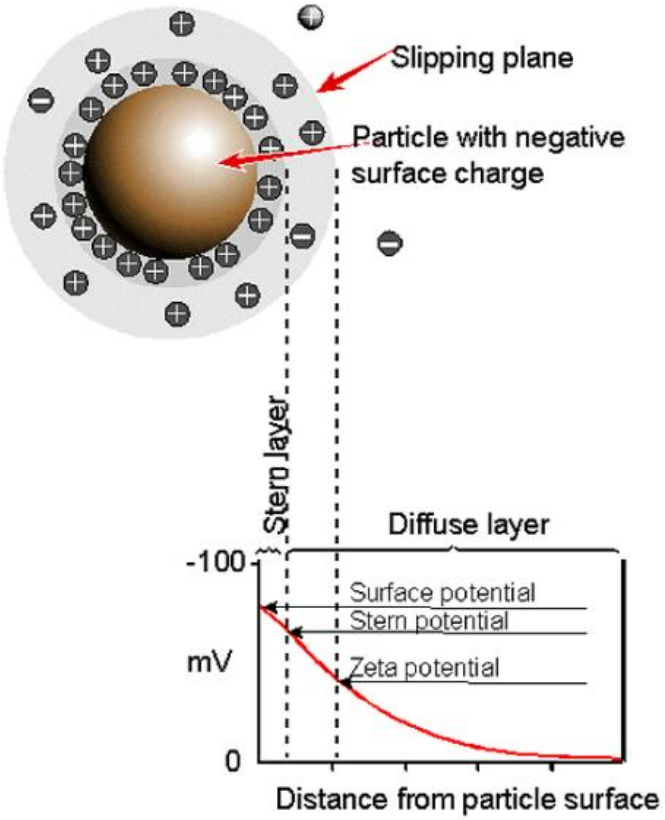


***Figure 4**: A diagram (Malvern Industries, 2015) showing the double electron layer. Two layers surround the molecule. An inner stern region and the outer diffuse region. Zeta potential defines the diffuse region. The greater the zeta potential the greater the size of the diffuse area. Interactions of particles with small diffuse areas can lead to aggregation with little force repelling other particles.*

High zeta potential indicates a high likelihood of repulsion, reducing the chances of aggregation, generally particles with <+30mv and >-30mv are stable in suspension. However, Zeta potential can be affected by pH (Vasile-Dan Hodoroaba, Wolfgang E  S Unger and Shard, 2020).

The zeta potential can be determined through gel electrophoresis, measuring the electrophilic mobility of molecules. The charge of the particles results in attraction of the oppositely charged electrode. The velocity of the particle when acting forces have reached equilibrium under a constant voltage gradient allows the zeta potential to be calculated.

$$U_e = \frac{2\varepsilon z f(\kappa a)}{3\eta} \quad (2)$$

Equation 3 (Clogston and Patri, 2010), the Henry equation of electrophoretic mobility ($U_e$). The zeta potential (z) can be calculated through rearrangement. η is the viscosity and f(κa) is Henry's constant, the ratio between the core of the molecule and the electron double layer.

The pH of a media can change the charge of the suspended LNPs. (Chakraborty and Panigrahi, 2020). Lowering the pH of a solution results in association to basic structures present on the surface of the molecule and protonation imparting a positive charge on the molecules. The reverse is true for low pH solutions and allows for the alteration of molecular characteristics based on the pH of the medium. The neutralization of the suspension, however, can induce aggregation as the zeta potential is too close to zero, reducing molecular ability for electrostatic repulsion, destabilizing the colloidal system. The thickness of the double electron layer (Debye length (κ)) is dependent on the media concentration (Malvern Industries, 2015). The greater the ionic strength of the media the greater the repression exerted on the double electron layer, reducing the electrostatic repulsion (Chakraborty and Panigrahi, 2020). This may lead to aggregation. The formulation of the media in suspension is a consideration as the greater the valency the more efficient it is at reducing the charge of the double electron layer.

### 1.6.3. SEC-MALS

The use of size-exclusion chromatography coupled with multi-angled light scattering (SEC-MALS) allows for the absolute determination of the particle size of the LNP formed without a standard curve needed for standalone SEC.

Characterising the molecular weight of the LNPs formed allows identification of unwanted aggregation, and the comparison between batches of LNPs. In addition, SEC-MALS can identify changes in LNP molar mass over time which may identify possible stability issues during storage. Size-exclusion chromatography (SEC) is a molecular separation technique, separating molecules based on their hydrodynamic sizes (Guillot et al., 2023). A column containing Porus beads, as seen in figure 5A, determines the rate at which molecules pass through. Small molecules get trapped within the beads resulting in the elution order of the largest molecules followed by the smallest (Guillot et al., 2023). SEC alone is a characterisation technique, however, to determine molar mass a standard curve must be formed using a sample of known weight is required. Calibration curves are dependent on the reference molecules being globular and inert. The calibration curve assumes the diffusion properties for the reference and sample molecules are similar, surface structures such as glycosylation can result in inaccurate results (Some et al., 2019).

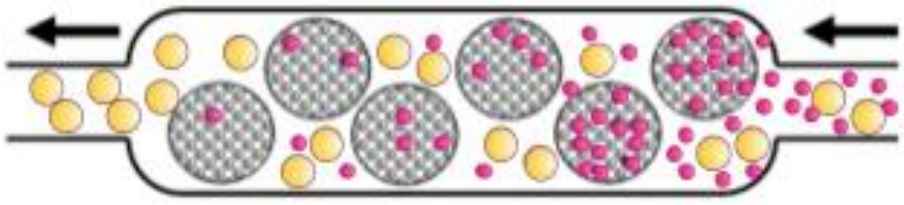

A

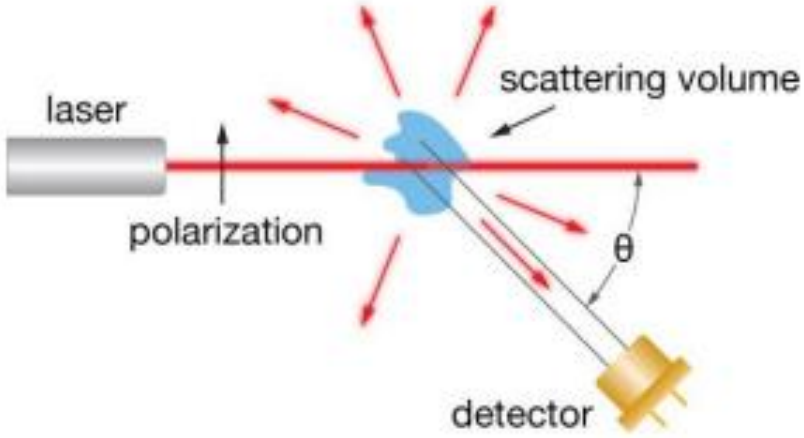


B

**Figure 5A**: A figure (Wyatt Technology corporation, 2019) showing the size exclusion column in SEC. Porus beads throughout the column entrap small molecules reducing their movement. Fractions are formed based on particles hydrodynamic diameter and their diffusion properties. The separation of molecules through size exclusion produces fractions of individual species. After the formation of a reference curve the elution time can be sed to determine the moelcular weight. **Figure 5B**: A diagram (Wyatt Technology corporation , 2019) higlighting the method in multi-angled light scattering (MALS) is used. A polarised laser is directed at the target sample and the intensity of the light relative to the angle of incident light is recorded, allowing the molecular lweight to be identified.

The adjacent use of multi-angled light scattering (MALS), as seen in figure 5B, produces an absolute measurement of molecular weight eliminating the need for a standard curve and allowing the production of live molecular weight data. MALS uses two detection systems $UV_{280}$ for absorbance and differential refractive index (dRI) detectors allowing the accurate determination of biophysical properties (Some et al., 2019). The refractive index of the sample is the determining factor for dRI detectors to calculate a samples concentration. Equation 1 allows the calculation of Mw using the proportions of light detected and angles in relation to the incident light.

$$M = \frac{R(0)}{Kc\left(\frac{dn}{dc}\right)^2} \quad (3)$$

The molar mass (M) of the sample is obtained using the reduced Rayleigh ratio R(0) is identified using the dRI detection angle intensities and extrapolated to 0. This is compared against the system constant (K), sample concentration (c) and the difference in refractive index of the sample and buffer (dn/dc) (Some et al., 2019).

SEC-MALS uses SEC for column separation. Separation to individual species allows for discrete and accurate testing of molecular species. Unlike the use of $UV_{280}$ for absorbance testing, dRI is a universal method for concentration identification as light scattering is unaffected by the presence of chromophores present on polysaccharides and sugars as seen in UV testing (Some et al., 2019).

### 1.6.4. Encapsulation Efficiency

The encapsulation efficiency of LNPs formulated is a quantitative measure of the success of mRNA uptake within the lipid matrices. The size and surface charge of the LNPs formulated are important for consistent formulation. The uptake of mRNA is another important factor relating to the efficacy and strength of LNP produced. Ribogreen assay is fluorescent dye that specifically binds to RNA. The intensity of fluorescence displayed is directly related to the RNA concentration. An aliquot of formulated LNP is taken and Ribogreen is added (Schober, Story and Arya, 2024). The fluorescence is detected using FLUOstar omega plate reader and represents only the free uncaptured RNA. Ribogreen cannot pass through or enter the lipid matrix (Schober, Story and Arya, 2024). After recording the free RNA intensity, a

detergent is used to degrade the LNP releasing the encapsulated RNA. Measuring the total RNA allows the percentage encapsulated to the obtained. Fluorescence assays are preferred over UV based absorbance analysis due to specific binding of the dye, which avoids the impact of excess buffer and broken inactive Damaged RNA which can influence the results gained (Schober, Story and Arya, 2024).

# 2. Conclusion

This review set out to identify key components and methods for producing and ensuring the consistency in encapsulation LNP molecules. LNP formulation has been identified as a delicate process which requires optimisation of surfactants to produce stable and uniform lipid nanoparticles which can effectively capture their required payload. Surfactants are important components to LNP physical and chemical characteristics directly influencing the size formed, their ability for endosomal escape and stability throughout serum circulation. These characteristics can be achieved through steric hinderance of PEGylation, or changes to rigidity via cholesterol.

LNP mixing protocols can vary depending on the constituents used and the mixing apparatus used. The herringbone mixer is an effective passive mixing method and one suitable to produce LNPs intended to carry nucleic based cargo. Active mixers offer greater control of mixing, as seen in pulse flow mixing, electricity is used to control the flow of two phases. This can result in the degradation RNA based cargo hence the staggered herringbone geometric mixing is the most suitable when dealing with delicate payloads such as mRNA.

Successful formulation relies on the constituents used; the payload must be kept in mind when choosing the method of mixing and testing the final formulation is key to change upstream components for consistent production. LNP testing is a key stage in their development, giving an insight into the potential behaviour expressed via the identification of PDI, zeta potential, molar mass and encapsulation efficiency. To achieve this, a number of distinct techniques such as dynamic light scattering, and SEC-MALs can be employed. Payload encapsulation can be measure through fluorescent based assays. The method of formulation

used for LNP production should be focused on the intended cargo to prevent potential adverse effects and the subsequent the parameters of the product should be thoroughgoingly characterised.

# 3. Acknowledgements

Firstly, I would like to thank my parents for the love, support and help they have given me throughout my years of education, especially A-levels and my time at university. Reaching the Master's level is something I once thought far beyond my ability, and I owe this achievement to their continued support.

I would like to thank my Dissertation supervisors, Prof. Stephen Harding and Dr. Shahwar Jiwani. Steve has been a great support and made his taught modules some of the most fun and engaging course I have taken, further piquing my interest of the subject. Shawar has been kind and welcoming as my manager, overseeing my placement at Sartorius Albumedix. I am very thankful for all her input she has offered or this paper.

Finally, I would like to thank Dr. Judith Wayte for helping me secure this placement at Sartorius Albumedix, and Sartorius Albumedix themselves for the opportunity to work with them.

# 4. References


**[1]** Anna Laura Nelson, Mancino, C., Gao, X., Choe, J.A., Chubb, L., Williams, K., Czachor, M., Marcucio, R., Taraballi, F., Cooke, J.P., Huard, J., Bahney, C. and Ehrhart, N. (2024). β-catenin mRNA Encapsulated in SM-102 Lipid Nanoparticles Enhances Bone Formation in a Murine Tibia Fracture Repair Model. *Bioactive Materials*, [online] 39, pp.273–286. doi:https://doi.org/10.1016/j.bioactmat.2024.05.020.

**[2]** Bhattacharjee, S. (2016). DLS and Zeta Potential – What They Are and What They Are not? *Journal of Controlled Release*, 235, pp.337–351. doi:https://doi.org/10.1016/j.jconrel.2016.06.017.

**[3]** Binici, B., Rattray, Z., Zinger, A. and Perrie, Y. (2024). Exploring the Impact of Commonly Used Ionizable and Pegylated Lipids on mRNA-LNPs: a Combined in Vitro and Preclinical Perspective. *Journal of Controlled Release*, [online] 377, pp.162–173. doi:https://doi.org/10.1016/j.jconrel.2024.11.010.

**[4]** Chakraborty, S. and Panigrahi, P.K. (2020). Stability of nanofluid: a Review. *Applied Thermal Engineering*, [online] 174, p.115259. doi:https://doi.org/10.1016/j.applthermaleng.2020.115259.

**[5]** Chauhan, I., Yasir, M., Verma, M. and Singh, A.P. (2020). Nanostructured Lipid Carriers: a Groundbreaking Approach for Transdermal Drug Delivery. *Advanced Pharmaceutical Bulletin*, [online] 10(2), pp.150–165. doi:https://doi.org/10.34172/apb.2020.021.

**[6]** Cho, E.J., Holback, H., Liu, K.C., Abouelmagd, S.A., Park, J. and Yeo, Y. (2013). Nanoparticle Characterization: State of the Art, Challenges, and Emerging Technologies. *Molecular Pharmaceutics*, 10(6), pp.2093–2110. doi:https://doi.org/10.1021/mp300697h.

**[7]** Clogston, J.D. and Patri, A.K. (2010). Zeta Potential Measurement. *Methods in Molecular Biology*, 697, pp.63–70. doi:https://doi.org/10.1007/978-1-60327-198-1_6.

**[8]** Feng, H. (2024). *Optimization of Lipif Nanoparticles (LNP) Formulations and Evaluation of the Product Stability* .

**[9]** Ferraresso, F., Strilchuk, A.W., Lih Jiin Juang, Poole, L.G., Luyendyk, J.P. and Kastrup, C.J. (2022). Comparison of DLin-MC3-DMA and ALC-0315 for siRNA Delivery to Hepatocytes and Hepatic Stellate Cells. *Molecular Pharmaceutics*, 19(7), pp.2175–2182. doi:https://doi.org/10.1021/acs.molpharmaceut.2c00033.

**[10]** Geall, A.J., Verma, A., Otten, G.R., Shaw, C.A., Hekele, A., Banerjee, K., Cu, Y., Beard, C.W., Brito, L.A., Krucker, T., O'Hagan, D.T., Singh, M., Mason, P.W., Valiante, N.M., Dormitzer, P.R., Barnett, S.W., Rappuoli, R., Ulmer, J.B. and Mandl, C.W. (2012). Nonviral delivery of self-amplifying RNA vaccines. *Proceedings of the National Academy of Sciences*, 109(36), pp.14604–14609. doi:https://doi.org/10.1073/pnas.1209367109.

**[11]** Guillot, A.J., Martínez-Navarrete, M., Garrigues, T.M. and Melero, A. (2023). Skin Drug Delivery Using Lipid vesicles: a Starting Guideline for Their Development. *Journal of Controlled Release*, 355, pp.624–654. doi:https://doi.org/10.1016/j.jconrel.2023.02.006.

**[12]** Haque, Md.A., Shrestha, A., Mikelis, C.M. and Mattheolabakis, G. (2024). Comprehensive analysis of lipid nanoparticle formulation and preparation for RNA delivery. *International Journal of Pharmaceutics: X*, [online] 8, p.100283. doi:https://doi.org/10.1016/j.ijpx.2024.100283.

**[13]** Johnson, T.J., Ross, D. and Locascio, L.E. (2002). Rapid Microfluidic Mixing. *Analytical Chemistry*, 74(1), pp.45–51. doi:https://doi.org/10.1021/ac010895d.

**[14]** Jung, H.N., Lee, S.-Y., Lee, S., Youn, H. and Im, H.-J. (2022). Lipid nanoparticles for delivery of RNA therapeutics: Current status and the role of *in vivo* imaging. *Theranostics*, 12(17), pp.7509–7531. doi:https://doi.org/10.7150/thno.77259.

**[15]** Jürgens, D.C., Deßloch, L., Porras-Gonzalez, D., Winkeljann, J., Zielinski, S., Munschauer, M., Hörner, A.L., Burgstaller, G., Winkeljann, B. and Merkel, O.M. (2023). Lab-scale siRNA and mRNA LNP Manufacturing by Various Microfluidic Mixing Techniques – an Evaluation of Particle Properties and Efficiency. *OpenNano*, [online] 12, p.100161. doi:https://doi.org/10.1016/j.onano.2023.100161.

**[16]** Lee, C.-Y., Chang, C.-L., Wang, Y.-N. and Fu, L.-M. (2011). Microfluidic Mixing: a Review. *International Journal of Molecular Sciences*, [online] 12(5), pp.3263–3287. doi:https://doi.org/10.3390/ijms12053263.

**[17]** Lee, Y., Jeong, M., Lee, G., Park, J., Jung, H., Im, S. and Lee, H. (2024). Development of Lipid Nanoparticle Formulation for the Repeated Administration of mRNA Therapeutics. *Biomaterials Research*, 28. doi:https://doi.org/10.34133/bmr.0017.

**[18]** Machado, B.A.S., Hodel, K.V.S., Fonseca, L.M. dos S., Mascarenhas, L.A.B., Andrade, L.P.C. da S., Rocha, V.P.C., Soares, M.B.P., Berglund, P., Duthie, M.S., Reed, S.G. and Badaró, R. (2021). The Importance of RNA-Based Vaccines in the Fight against COVID-19: An Overview. *Vaccines*, [online] 9(11), p.1345. doi:https://doi.org/10.3390/vaccines9111345.

**[19]** Malvern Industries (2015). *Zeta potential: an Introduction in 30 Minutes* . [online] Malvern Industries . Available at: file:///C:/Users/Joe/AppData/Local/Microsoft/Olk/Attachments/ooa-ede8efd9-1d59-4d4b-9f66-b08172b99fec/ced8b7c85ac15d0200d2006aa35818098e3008cf99e0f204ec4b47d7c0989bbf/ZetaPotential-Introduction-in-30min-Malvern.pdf.

**[20]** Malvern Instruments (2006). *What Is the Henry Equation?* [online] LSU Macromolecular Strudies Group . Available at: https://macro.lsu.edu/HowTo/MALVERN/FAQ_HTML/what_is_the_henry_equation/what_is_the_henry_equation_.htm.

**[21]** Malvern Instruments (2017). *Dynamic Light Scattering: an Introduction in 30 Minutes* . [online] Malvin Instruments . Available at: https://www.research.colostate.edu/wp-content/uploads/2018/11/dls-30min-explanation.pdf.

**[22]** Marjorie and Luís Alexandre Muehlmann (2024). Characteristics and Preparation of Solid Lipid Nanoparticles and Nanostructured Lipid Carriers. *Journal of Nanotheranostics*, [online] 5(4), pp.188–211. doi:https://doi.org/10.3390/jnt5040012.

**[23]** Mehta, M., Bui, T.A., Yang, X., Aksoy, Y.A., Goldys, E.M. and Deng, W. (2023). Lipid-Based Nanoparticles for Drug/Gene Delivery: an Overview of the Production Techniques and Difficulties Encountered in Their Industrial Development. *ACS Materials Science Au*, 3(6). doi:https://doi.org/10.1021/acsmaterialsau.3c00032.

**[24]** Musielak, E., Feliczak-Guzik, A. and Nowak, I. (2022). Synthesis and Potential Applications of Lipid Nanoparticles in Medicine. *Materials*, 15(2), p.682. doi:https://doi.org/10.3390/ma15020682.

**[25]** Nguyen, T.-T.-L. and Duong, V.-A. (2022). Solid Lipid Nanoparticles. *Encyclopedia*, [online] 2(2), pp.952–973. doi:https://doi.org/10.3390/encyclopedia2020063.

**[26]** Ripoll, M., Martin, E., Enot, M., Robbe, O., Rapisarda, C., Nicolai, M.-C., Deliot, A., Tabeling, P., Authelin, J.-R., Nakach, M. and Wils, P. (2022). Optimal self-assembly of lipid nanoparticles (LNP) in a ring micromixer. *Scientific Reports*, [online] 12(1), p.9483. doi:https://doi.org/10.1038/s41598-022-13112-5.

**[27]** Roces, C.B., Lou, G., Jain, N., Abraham, S., Thomas, A., Halbert, G.W. and Perrie, Y. (2020). Manufacturing Considerations for the Development of Lipid Nanoparticles Using Microfluidics. *Pharmaceutics*, 12(11), p.1095. doi:https://doi.org/10.3390/pharmaceutics12111095.

**[28]** Schober, G.B., Story, S. and Arya, D.P. (2024). A Careful Look at Lipid Nanoparticle characterization: Analysis of Benchmark Formulations for Encapsulation of RNA Cargo Size Gradient. *Scientific Reports*, [online] 14(1), p.2403. doi:https://doi.org/10.1038/s41598-024-52685-1.

**[29]** Some, D., Amartely, H., Tsadok, A. and Lebendiker, M. (2019). Characterization of Proteins by Size-Exclusion Chromatography Coupled to Multi-Angle Light Scattering (SEC-MALS). *Journal of Visualized Experiments*, (148). doi:https://doi.org/10.3791/59615.

**[30]** Soni, S., Maheshwari, R.K. and Sah, A.K. (2024). Nanostructured Lipid Carrier: Beneficial Role in Oral Drug Delivery System. *BioNanoScience*, 14(4), pp.3988–4005. doi:https://doi.org/10.1007/s12668-024-01416-x.

**[31]** Stetefeld, J., McKenna, S.A. and Patel, T.R. (2016). Dynamic Light scattering: a Practical Guide and Applications in Biomedical Sciences. *Biophysical Reviews*, 8(4), pp.409–427. doi:https://doi.org/10.1007/s12551-016-0218-6.

**[32]** Stroock, A.D., Dertinger, S.K.W., Ajdari, A., Mezić, I., Stone, H.A. and Whitesides, G.M. (2002). Chaotic Mixer for Microchannels. *Science*, [online] 295(5555), pp.647–651. doi:https://doi.org/10.1126/science.1066238.

**[33]** Suh, Y.K. and Kang, S. (2010). A Review on Mixing in Microfluidics. *Micromachines*, [online] 1(3), pp.82–111. doi:https://doi.org/10.3390/mi1030082.

**[34]** Suk, J.S., Xu, Q., Kim, N., Hanes, J. and Ensign, L.M. (2016). PEGylation as a Strategy for Improving nanoparticle-based Drug and Gene Delivery. *Advanced Drug Delivery Reviews*, [online] 99, pp.28–51. doi:https://doi.org/10.1016/j.addr.2015.09.012.

**[35]** Vasile-Dan Hodoroaba, Wolfgang E S Unger and Shard, A.G. (2020). *Characterization of Nanoparticles : Measurement Processes for Nanoparticles*. Amsterdam Elsevier.

**[36]** Wang, J., Ding, Y., Chong, K., Cui, M., Cao, Z., Tang, C., Tian, Z., Hu, Y., Zhao, Y. and Jiang, S. (2024). Recent Advances in Lipid Nanoparticles and Their Safety Concerns for mRNA Delivery. *Vaccines*, [online] 12(10), p.1148. doi:https://doi.org/10.3390/vaccines12101148.

**[37]** Williams, M.S., Longmuir, K.J. and Yager, P. (2008). A Practical Guide to the Staggered Herringbone Mixer. *Lab on a chip*, [online] 8(7), pp.1121–9. doi:https://doi.org/10.1039/b802562b.

**[38]** Wyatt Technology corporation (2019). *SEC-MALS for Absolute Biophysical Characterization* . [online] https://www.wyatt.com/library/application-notes/by-technique/sec-mals.html. Available at: https://wyattfiles.s3-us-west-2.amazonaws.com/literature/white-papers/WP1615-SEC-MALS-for-absolute-biophysical-characterization.pdf.

**[39]** Yavuz, A., Coiffier, C., Garapon, C., Gurcan, S., Monge, C., Exposito, J.-Y., Arruda, D.C. and Verrier, B. (2023). DLin-MC3-Containing mRNA Lipid Nanoparticles Induce an Antibody Th2-Biased Immune Response Polarization in a Delivery Route-Dependent Manner in Mice. *Pharmaceutics*, [online] 15(3), p.1009. doi:https://doi.org/10.3390/pharmaceutics15031009.


# Formulation and Biophysical Characterisation of Poly (A)-loaded Lipid Nanoparticles – Effects of Recombumin® on Physiochemical Properties

University of Nottingham

MRes Biomolecular Technology

Joseph Turpin

September 2025

Supervisors:

Professor Stephen Harding – University of Nottingham

Dr. Shahwar Jiwani – Sartorius Albumedix

# Contents

# 1. Abstract

Lipid nanoparticles (LNPs) are small (less than a micron), lipid-based entities surrounding nucleotide-based agents sauch as mRNA as seen in mRNA vaccine developed by Pfizer and BioNTech during COVID-19. Use of ionisable lipids, phospholipids, cholesterol and PEGylated lipids forms a stable complex, capable of shielding delicate cargo (e.g a nucleotide).

During this project, we used a staggered herringbone mixing chip to create LNPs. Herringbone chip provides chaotic mixing and provides uniform diffusion which leads to uniform LNP particle synthesis. The LNPs thus produced were tested for their biophysical characteristics using dynamic light scattering (DLS) to determine their hydro dynamic radius, Zeta (ζ)-potential to measure their surface charge and Size Exclusion Chromatography coupled with Multi-Angled Light Scattering (SEC-MALS) to calculate the molar mass of the samples produced. Recombinant human albumin (rHA) Recombumin® Prime and Recombumin® Elite, products of Sartorius Albumedix Limited, were added to the LNP samples to test for LNP interaction and determine their effect on the suitability of the assay to detect the LNP. Increase in LNP size and reduction in surface charge, with the addition of albumin indicated the influence of albumin on the hydrodynamical properties of LNPs. SEC-MALS based investigations gave an indication of some interactions between LNP and albumin. On that account, it was inferred that DLS and SECMALs provided suitable baseline information about the biophysical properties of LNPs.

However, given the time frame of this work, it was not identified if the interaction between the two moieties were real and if they would affect overall functionality of the LNP.

# 2. Introduction

Lipid nanoparticles (LNPS) are lipid-based encapsulation structures, up to 1000nm in size and used in the transport of drugs and other therapeutic agents such as mRNA (Mehta et al., 2023). The use of LNPs during the COVID-19 pandemic was pertinent for successful delivery of mRNA cargo to desired target sites. Previous vaccination methods have included the use of inactive viral samples to induce the production of immunological cells against viral epitopes (Mehta et al., 2023, Pallesan et al*.,* 2017). During the COVID-19 pandemic the application of LNPs and nucleotide-based therapeutics in modern vaccine development was showcased through the Pfizer-BioNTech and Moderna mRNA vaccines. Unfortunately, this is only applicable when key epitopal proteins are well defined prior to vaccine development as seen with the structural spike protein of the coronavirus (Nail Minigulov et al., 2024).

Under normal physiological conditions nucleotide-based payloads such as mRNA are prone to degradation due to unfavourable pH environments and temperatures in addition to detection by the reticuloendothelial system (RES) (Mehta et al., 2023). Viral vectors and simple LNP structures, such as adenovirus and liposomes, have previously been used for mRNA transport, however, these methods encountered problems of longevity and stability, resolved through the development of modern LNPs (Mehta et al., 2023). Delivery through the adenovirus has the largest possibility of inducing an immune response when compared to other delivery mechanisms. Induction of the RES system results in the degradation of the payload and reduced therapeutic effectiveness in addition to limited usage per patient as due to resulting immune responses to the foreign species (Haque et al., 2024). Liposomes on the other hand, are lipid based,

forming a fluid lipid-bilayer a payload can be encapsulated. Liposomes have simple structures that are dependent on the lipid used and limited use of active surface components, such as cholesterol, which can aid the stability of the vesicle formed. These delivery mechanisms are less effective than modern LNPs such as solid lipid nanoparticles (SLNs) and nanostructured lipid carriers (NLCs). Surfactants such as ionizable lipids, cholesterol, phospholipids and PEGylated lipids allow for control over the efficiency of cargo encapsulation, payload release and evasion from the RES immune pathway (Chauhan et al., 2020).

Structural surfactants, such as ionisable lipids, are one of the determining factors to the bioavailability, encapsulation efficiency as well as the biophysical properties of the LNP produced. In the formulation of LNPs with nucleotide-based cargo, ionisable lipids are key components which are designed to bind to the cargo through polar interactions. At physiological environments where pH ~7.4, ionisable lipids are stable (Wang et al., 2024) a reduction in environmental pH due the presence of endosomes allow extracellular uptake of cargo into the cytoplasm. At a low pH, a positive charge is induced upon the ionisable lipids, resulting in the protonation of the endosome. This protonation results in the formation of an osmotic gradient, stimulating the transfer of the payload from the LNP carrier to the target cell (Haque et al., 2024). The incorporation of polyethylene glycol (PEG) chains on LNP structures aid by imparting 'stealth' like properties (Suk et al., 2016). The large structural conformations of the PEG lipids prevent the binding of RES signalling molecules known as opsonin's via steric hinderance. Without the initiation via opsonin's, the RES system is unable to detect and activate monocyte responses to LNPs and increasing the survival chance of the payload.

Phospholipids and cholesterol are examples of structurally supporting lipids. DSPC is an example of a phospholipid used for to its high melting point due to the presence of double bonds. These double bonds allow for a greater amount of stress exerted onto the complex (Jung et al., 2022). Hence the addition of phospholipids in the nanostructured lipid carriers prevents degradation of the complex in unfavourable environments, increasing the serum half-life. Early development of LNPs previously saw phospholipids as a major component within the LNP matrix, now usually contributing to only 10% to the structural formation in favour for the biologically safe ionisable lipids (Jung et al., 2022). On the other hand, cholesterol is present in the smallest molar percentage, controlling the molecular rigidity of the lipid complex. These structural surfactants aid in maintaining a sturdy but fluid lipid complex, increasing the biodistribution of the transported agent and extending the LNPs serum half-life (Wang et al., 2024).

Albumin (HA) is a key transporter protein within the body. HA is a 585 amino acids long single chain protein which forms 50% of all proteins within human plasma (Caraceni, Tufoni and Bonavita, 2013). Albumin has a negative total net charge molecule, allowing the attraction and binding to of positively charged molecules and hydrophobic molecules such as cholesterol (Johnson et al., 2022). The addition of Albumin to other delivery systems have been proven to aid in the stability of the delivery system and increase the serum half-life. However, dedicated albumin binding domains must be present on the vector for successful albumin binding to occur (Caraceni, Tufoni and Bonavita, 2013).

In this study we aimed to develop and characterise LNPs as described in literature by using synthetic nucleic acid and mixture of lipids (Jürgens et al., 2023). Light scattering methods were employed to identify successful LNP preparations and

their hydrodynamic properties. We used DLS, to determine particle size distribution and zeta potential, and SEC-MALS on LNP on their own and a mixed system where LNP were mixed with Recombumin® Prime and Recombumin® Elite.

# 3. Materials and Methods

## 3.1 Formulation of Lipid Nano particles (LNP)

LNP were prepared by mixing organic and aqueous phases (REF). The organic phase components included ionisable lipid (6Z,9Z,28Z,31Z)-Heptatriaconta-6,9,28,31-tetraen-19-yl 4-(dimethylamino) butanoate (D-Lin-MC3-DMA, CAYMAN Chemical Company, USA), phospholipid 1,2-distearoyl-sn-glycero-3-phosphocholine (DSPC,Avanti Research, USA), cholesterol (Merck, Germany) and 1,2-dimyristoyl-rac-glycero-3-methoxypolyethylene glycol-2000 (DMG-PEG2000, Avanti Research, USA). These components were diluted in absolute ethanol to form 10mM stock solutions. All components were further diluted in absolute ethanol to get a working dilution of 1mM. The aqueous phase containing 10ug/mL of Poly (A) tails (Sigma Aldridge, USA), was dissolved in a 25mM sodium acetate buffer (Sigma Aldridge, USA) (pH 12).

A staggered herringbone mixing chip (microfluidic ChipShop, Germany) was used to combine the two phases. The syringes and the mixing chip were connected using 0.5 mm PTFE tubing (microfluidic ChipShop, Germany) with 0.76mm silicon tubing connecting the herringbone 1/16” adapter luers (microfluidic ChipShop, Germany) and 0.5mm syringe adapter luer connectors (microfluidic ChipShop, Germany) (Figure 1). The system was cleaned with absolute ethanol and water through their respective inlets to flush through bubbles and any previously left material.

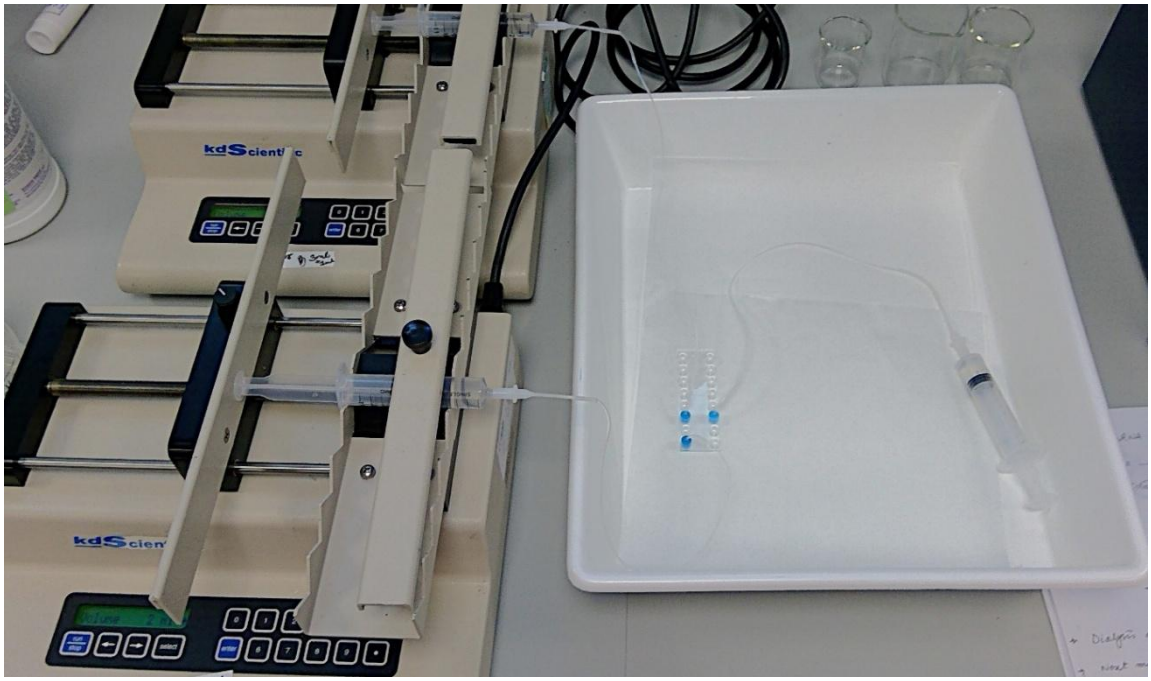

Figure 1: Visual representation of the staggered herringbone mixing set-up to produce LNPs. One pump for each of the two phases in the LNP production. Together they were set to dispense in a 3:1 ratio of aqueous: organic phase.

D-Lin-MC3-DMA, DSPC, Chol, and PEG were mixed in a ratio of 50:10:38.5:1.5 respectively to produce the organic phase. A flow rate ratio of 3:1 aqueous to organic phase and a total flow rate of 5mL/min was used. The total flow rate was controlled using mechanical syringe pumps (KD scientific, USA) pushing the 10ml syringes (Terumo, Japan) for each inlet. The final mixture was also collected in 10ml syringes (Terumo, Japan).

The collected LNP solution was dialysed using a 3-12 mL 10kDa dialysis cassette (ThermoFisher Scientific, USA) suspended in 1x PBS (pH 7.0) (950 mg/L phosphate 10mM, 201 mg/L KCl 2.68 mM, 8,120 mg/L NaCl 140 mM, ThermoFisher scientific, USA) overnight.

## 3.2 Formulation of LNP with Albumin

Post dialysis, LNPs were mixed with recombinant human albumin (rHA), Recombumin® Prime and Recombumin® Elite (Sartorius Albumedix Limited, UK). Each rHA was tested at 1 g/L and 5 g/L with LNP.

## 3.3 DLS measurements

Dynamic light scattering calculates size and zeta potential of the suspended particles in a solution using Quasi-Elastic Light Scattering. The hydrodynamic radius is measured using the Stokes-Einstein equation (1).

$$d(H) = \frac{kT}{3\pi\eta D} \quad (1)$$

Where $d(H)$ is the hydrodynamic diameter, $k$ the Boltzman distribution, $D$ is the translation diffusion coefficient, $T$ the absolute temperature and $\eta$ the viscosity.

Particle size, polydispersity and zeta potential were all tested using Zetastar DynaPro (Waters, WYATT Technology, USA) at 25°C. The LNP sample dilutions (1:2, 1:4, 1:8, 1:10, 1:20, 1:40) were prepared in PBS (pH 7.0) (Thermo Fisher Scientific, USA) and water. Two different cuvettes were compared for zeta potential measurements. A 45µL quartz cuvette (Waters Wyatt Technology, USA) was used to test Size and Zetapotential. A dip cell (Waters Wyatt Technology, USA) was used for Zeta potential measurements only. Each sample was measured three times and the results presented as the mean standard deviation ( ±SD). A scattering angle of 90° was used for size and polydispersity measurements and a scattering angle was 163.5° was used for zeta potential. The data was collected by DYNAMICS 8.4 using values from cumulant radius, based on number-based size distribution.

However, individual radii instead of cumulative radius were used when LNP and albumins were mixed together. This is because strong signals from albumin could superimpose other components in the mixture and could skew the overall results.

## 3.4 SEC-MALS

Size exclusion chromatography paired with multi-angled light scattering (SEC-MALS) was used to separate and identify species physical properties and concentration of LNP samples including control and mixed with 1 g/L and 5 g/L of human albumin 1 (rHA Recombumin® Prime) and human albumin 2 (rHA Recombumin® Elite). Species separation was performed with an Agilent 1260 Bio-inert high pressure liquid chromatography (HPLC) using a 7.8x300mm Waters GTX 2000Å column with a 4.8x30mm guard column which were heated to 30°C. The Diode Array Detection system (DAD), with a slit width of 10nm recorded absorbance at 350, 280, 260 and 220nm. Background subtraction at 600nm (averaged over ±50 nm) was applied for the 350nm reading, and the background subtraction at 360nm (averaged over ±50 nm) was applied for the 280,260, and 220nm. Light scattering intensity was measured using an ambient Wyatt Dawn Neon Multiangle light scattering system. Concentration was determined with a Wyatt Optilab Neon differential refractive index (dRI) detector, and inline DLS measurements were performed using a connected Wyatt Zetastar.

# 4. Results

## 4.1 DLS and Zeta potential

### *4.1.1 Hydrodynamic radii of LNP*

LNPs were present as a single species in the formulation, therefore, hydrodynamic radius of LNPs was calculated using cumulant fit. LNPs were tested in the concentration range of (1:2 to 1:40) in 1XPBS (pH 7.0) (Table 1, Figure2). Figure 2 shows an exponential increase in the radius (nm) as concentration of LNP increases. An overall average radius was 124.5±9.4 nm, mostly ranging from 116.7±4.1 nm at the lowest concentration to 142.5±4.3 nm at the highest concentration. Presence of single peak and low PDI indicated that the LNPs were stable with little to no aggregation Table 1.

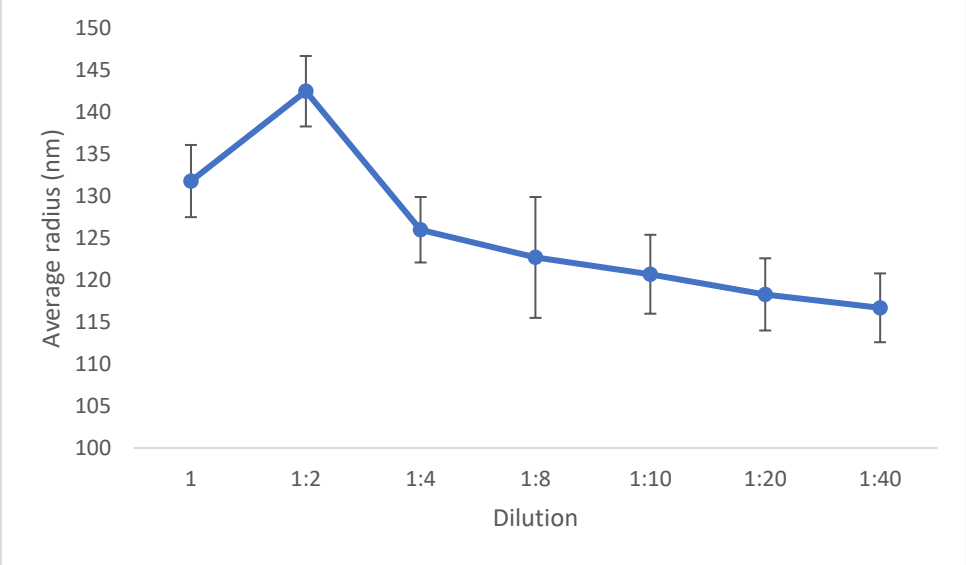


Figure 2: Hydrodynamic radius (nm) of LNPs post-dialysis in 1x PBS (pH 7.0) and diluted using 1x PBS (pH 7.0), for each dilution n=1 ±SD.

Table 1:The average radius ± SD and polydispersity of a series of LNP dilution (1 to 1:40) in 1x PBS (pH 7.0).

| Dilution | Radii ± SD (nm) | PDI (%) |
|---|---|---|
| 1 | 131.8±4.2 | 17.8 |
| 1:2 | 142.5±4.3 | 15.89 |
| 1:4 | 126±3.9 | 8.06 |
| 1:8 | 122.7±7.2 | 10.04 |
| 1:10 | 120.7±4.7 | 10.49 |
| 1:20 | 118.3±4.3 | 10.46 |
| 1:40 | 116.7±4.1 | 10.48 |

Figure 3 shows average radius (nm) of LNP when diluted from 1:2 to 1:40 in water, 0.1X and0.5X PBS (pH 7.0) compared against the initial results of LNPs in 1XPBS (pH 7.0). Overall average radii of LNP formulations diluted in water, had the largest average radius of 131.5±7.4 nm, with the second largest radii recorded, 128nm±6.2 in 0.1XPBS (pH 7.0). On the other hand, 0.5XPBS (pH 7.0) and 1XPBS (pH 7.0) produced the smallest average radii of 118.7nm±7.7 and 124nm±9.4 respectively.

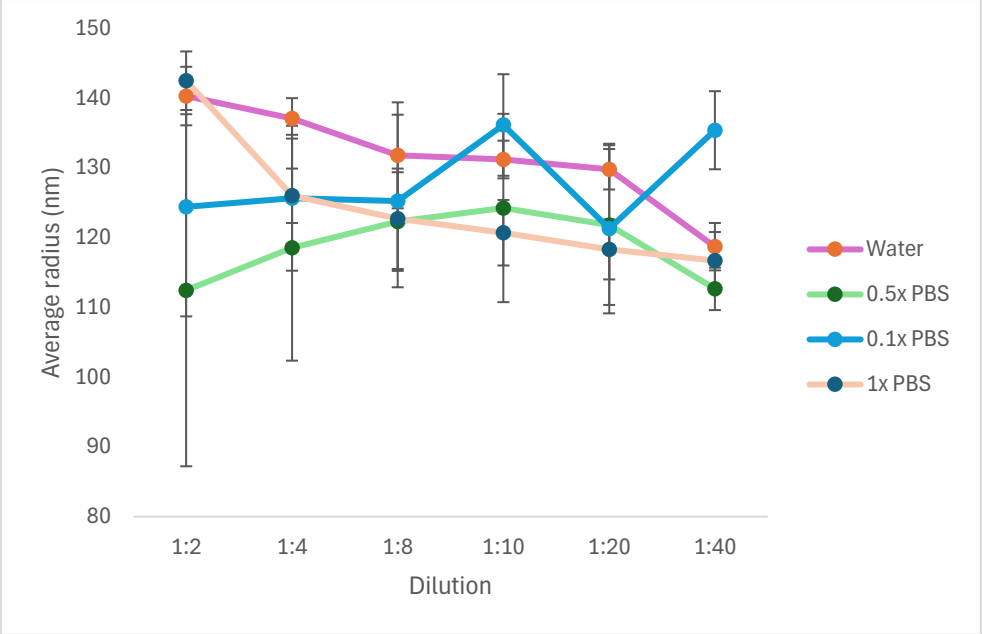


Figure 3: A graph showing the comparison in hydrodynamic radius between LNP dilutions in 1x PBS (pH 7.0), 0.5x PBS (pH 7.0), 0.1x PBS (pH 7.0) and water in a series of dilutions 1:2-1:40. *Where possible (0.5x PBS (pH 7.0) and 0.1x PBS (pH 7.0)) n=3 ±SD, otherwise n=1 ±SD based of cumulant average.*

Solvent salt concentration determines the intermolecular interactions of colloidal solution. At low salt concentrations (such as 0.1X PBS, pH 7.0) molecules have less repulsion to intermolecular interactions as a result of reduced charge shielding. Whereas at high salt concentrations, e.g., 1XPBS (pH 7.0), the molecule can dehydrate because of water competition with salt in solution. Both too much and too little salt can result in increased aggregation affecting the hydrodynamic radius produced (Francis et al., 2025).

0.5XPBS (pH 7.0) and 1XPBS (pH 7.0) share similar trends between average radii and concentration between 1:8-1:40. In comparison, water, as seen in Table 2, has an average radius 9-12nm larger than 1XPBS (pH 7.0) in most concentrations.

Table 2: A Table showing the values of the average diameters (nm) and ±SD of LNPs in descending concentration of PBS (pH 7.0) buffers across a dilution range of 1:2-1:40

| Dilution | Average Radius (nm) ±SD | | | |
|---|---|---|---|---|
| | 1x PBS (pH 7.0) | 0.5x PBS (pH 7.0) | 0.1x PBS (pH 7.0) | Filtered water |
| 1:2 | 142.5 ±4.2 | 112.5 ±25.2 | 124.4 ±15.7 | 140.3 ±4.2 |
| 1:4 | 126 ±3.9 | 118.5 ±16.2 | 125.7 ±10.4 | 137.1 ±2.9 |
| 1:8 | 122.7 ±7.2 | 122.3 ±7.1 | 125.3 ±12.4 | 131.8 ±7.6 |
| 1:10 | 120.7 ±4.7 | 124.3 ±13.5 | 136.2 ±7.3 | 131.2 ±2.7 |
| 1:20 | 118.3 ±4.3 | 121.8 ±11.5 | 121.3 ±12.2 | 129.8 ±2.9 |
| 1:40 | 116.7 ±4.1 | 112.7 ±3 | 135.4 ±5.6 | 118.7 ±3.4 |
| Average | 124.5±9.4 | 118.7±7.7 | 128.0±6.2 | 131.5±7.4 |
| Standard deviation | 9.41 | 5.07 | 6.20 | 7.43 |

*4.1.2 Zeta (ζ) potential or Surface charge of LNPs*

ζ-potential or surface charge measurement is one of the important tools to determine colloidal stability. It helps to recognise how a suspended molecule maintains its integrity in the given solution conditions such as salt concentration, pH and temperature. ζ-potential was performed using a ZetaStar DynaPro (Waters, WYATT Technology, USA) with 45 µL cuvette and a Dip-cell (forming an electrophoretic environment).

Initial testing with ζ-potential showed 1x PBS (pH 7.0) to be an unsuitable diluent as the salt concentration was too high. No results could be collected due to the formation of bubbles in the sample. PBS (pH 7.0) was diluted to 0.5X and 0.1X and tested to determine the most suitable diluent for ζ-potential data collection.

Figure 4 shows the zeta potential of LNPs diluted in filtered water, 0.5x PBS (pH 7.0), and 0.1x PBS (pH 7.0). it was observed that 0.5XPBS (pH 7.0) to have an average surface charge of -24.24±19.3 mV, the highest charge of all three solvents. Both water and 0.1XPBS (pH 7.0) recorded similar ζ-potentials of -19.9±5.5 mV and -16.1±4.4 mV.

Figure 4 shows 0.5x PBS (pH 7.0) (green) to produce inconsistent ζ-potentials, with no results produced at the 1:4 dilution as a result of high salt concentrations. This was considered as the least suitable buffer. LNPs diluted in both 0.1x PBS (pH 7.0) and filtered water produced similar zeta potential results ranging from ~-25 mV at the lowest concentration to ~-10 mV at the highest concentration. The similarity of the curves indicated both diluents have similar surface charge.

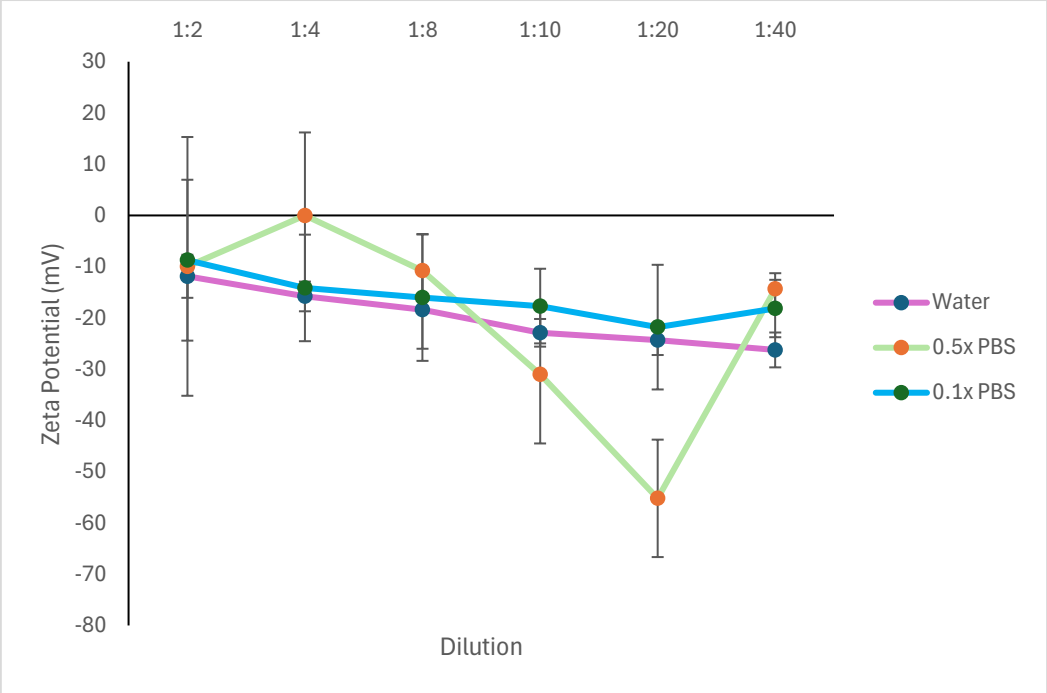


Figure 4: A graph showing the comparison between the Zeta potential of LNPs in a series of dilutions, diluted with Water, 0.5x PBS (pH 7.0), and 0.1x PBS (pH 7.0). Where possible (0.5x PBS (pH 7.0) and 0.1x PBS (pH 7.0)) n=3 ±SD, otherwise n=1 ±SD based of cumulant average.

Use of 0.1x PBS (pH 7.0) is more reliable for surface charge measurements as presence of correct salt concentration produces one of the highest zeta potential values which represents good stability of the LNPs. The presence of strong electrostatic repulsion between like particles reduces the chance of aggregation (Figure 3). A small zeta potential in the presence of too much salt or too little salt increases the possibility of aggregation within the sample.

*4.1.3 Size of Albumin* Recombumin® *Prime and* Recombumin® *Elite.*

rHA (Recombumin® Prime and Recombumin® Elite) sizes and polydispersity were tested at their stock concentrations (200 g/L Recombumin® Prime, 100 g/L Recombumin® Elite) and at 5 g/L and 1 g/L diluted in 1x PBS (pH 7.0). The size and polydispersity of these concentrations can be seen in Figure 5 and Table 3.

It was observed that at stock concentration, both proteins had the smallest average radii, 3.0±0.005 nm and 2.0±0.001 nm respectively. 1 g/L rHA Recombumin® Prime produced the greatest average radii of 4.1±0.8 nm. All other rHA samples (1 and 5 g/L rHA Recombumin® Elite and 5 g/L rHA Recombumin® Prime) had the same average radius of 3.6±0.0 nm.

Stock concentrations of rHA Recombumin® Elite was found to be 1 nm smaller than rHA Recombumin® Prime. Interestingly, both rHA Recombumin® Prime and Recombumin® Elite have the same particle size of 3.5±0 nm at 5 g/L despite their initial sizes having a 1 nm difference at stock concentrations. At 1 g/L rHA Recombumin® Prime is seen to have the greatest increase in size 4.1±0.8 nm as well as polydispersity (14.75%), 0.5 nm larger in size and nearly a 7 times larger polydispersity than 1 g/L rHA Elite. However, this is likely to be a an error occuring during sample forumlation.

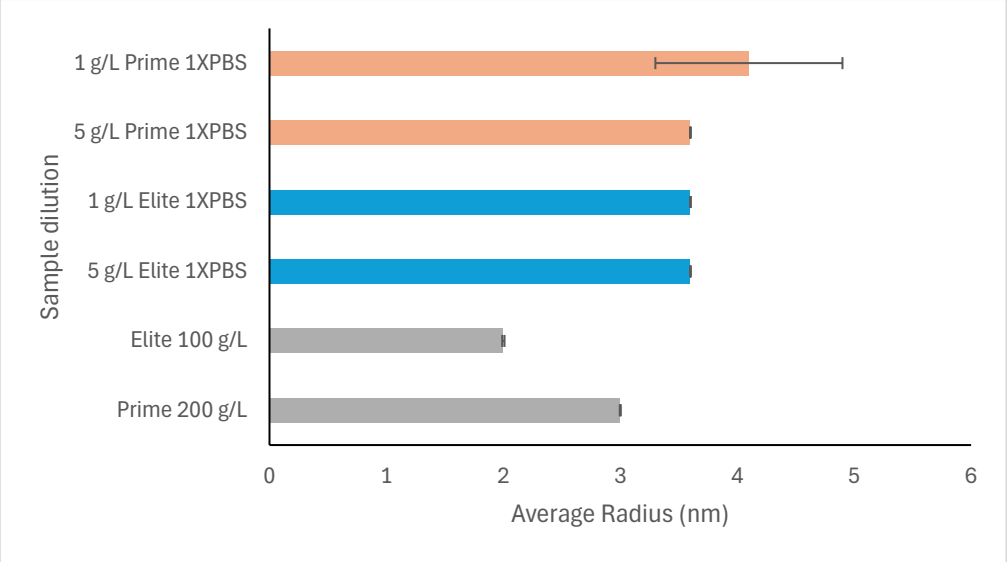


Figure 5: Bar chart showing the average radii of rHA Recombumin® Prime and Recombumin® Elite at their native concentrations (200 g/L and 100 g/L respectively) and the concentrations intended for LNP trialling (1 g/L and 5 g/L), diluted in 1XPBS (pH 7.0). During testing n=1 ±SD.

*Table 3: Table displaying the average radius± SD of recombine Recombumin® Prime and Recombumin® Elite and their polydispersity at their stock concentration (rHA* Recombumin® *Prime — 200 g/L and rHA* Recombumin® *Elite – 100 g/L), 1 g/L in 1x PBS (pH 7.0) and 5 g/L 1x PBS (pH 7.0). During testing n=1 ±SD.*

| Dilution | Recombumin® Prime | | Recombumin® Elite | |
|---|---|---|---|---|
| | Radii ± SD | PDI (%) | Radii ± SD | PDI (%) |
| Stock | 3.0 ± 4.6x10$^{-03}$ | 6.25 | 2.0 ± 9.9x10$^{-03}$ | 2.97 |
| 1 g/L | 4.1 ± 0.8 | 14.75 | 3.6 ± 0 | 2.87 |
| 5 g/L | 3.6 ± 0 | 5.31 | 3.6 ± 0 | 3.79 |

### *4.1.4 Mixing of LNP with Recombumin® albumins*

To identify the effect rHA had on LNP size, LNPs were mixed with rHA Recombumin® Prime and Recombumin® Elite at 5 g/L and 1 g/L in 1XPBS (pH 7.0), and the subsequent samples were measured for their average radius, polydispersity and zeta ζ-potential.

Mixing rHA Recombumin® Prime and Recombumin® Elite at 5 g/L and 1 g/L gave two distinct peaks when tested with DLS as (Figure 6). Peak one ranges in size

between 1-10 nm indicating the presence of rHA when compared to Table 3. Size of LNP (Peak 2) was ~131.8nm. The addition of rHA resulted in slight shift in radius of LNPs to the right (Peak 3 in Figure 6) than that of the average LNP radius in the absence of albumin (Table 1).

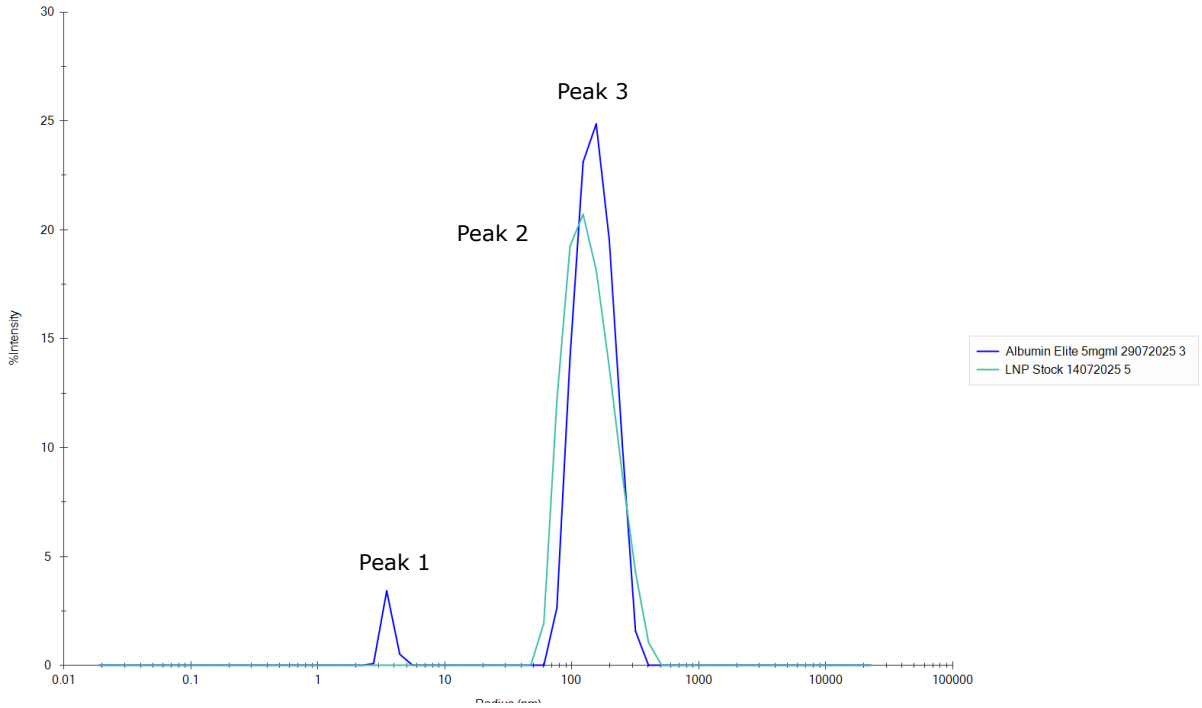


Figure 6: A %intensity graph (DYNAMICS 8.4) showing the intensity of scattered light of mixed sample 5 g/L rHA *Recombumin*® Elite diluted with 1XPBS (pH 7.0) and LNP. Two distinct peaks can be seen, peak 1 – rHA *Recombumin*® Elite and peak 2 – LNP mixed with rHA *Recombumin*® Elite. This graph shows single measurements for clarity.

Figure 7 shows the average hydrodynamic radius (nm) of LNPs when mixing with Recombumin® Prime and Recombumin® Elite at 1 g/L and 5 g/L and compared against LNP control. The average hydrodynamic radius of LNPs increased when rHA was added.

LNP without rHA had a radius of 131.8±4.2 nm (Figure 7). Addition of 1 and 5 g/L rHA Recombumin® Prime resulted in an increase in diameter, with average radii of 144.8±7 nm and 152.4±8.5 nm, respectively. Formulation with rHA Recombumin®

Elite (1 g/L) had the largest average diameter of 174.1±36.6 nm. Increase in the size of LNP could be due to binding of some of the albumin to the LNPs.

LNP radii was at its largest when mixed with rHA Recombumin® Elite for both 1 and 5 g/L.

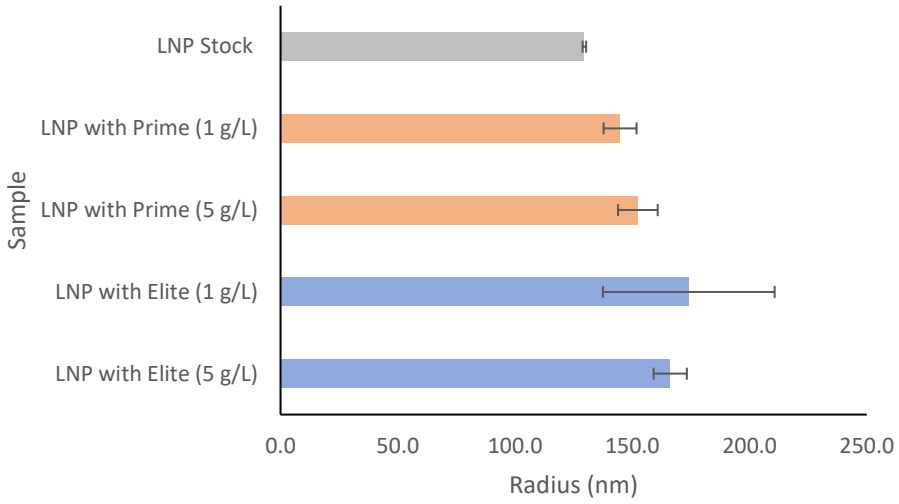


Figure 7: A graph showing the average hydrodynamic radii, collected through DLS, of LNP when mixed with 1g/L and 5g/L human albumin Recombumin® Prime and Recombumin® Elite. The data produced n=3 ±SD (excluding LNP Stock where n=1 ±SD)

Figure 8 shows the polydispersity of the LNP and rHA Recombumin® mixed samples. LNP without albumin sample has a PDI of 17.8±2.9%, the smallest of all samples shown in Figure 8. Increase in PDI with the addition of rHA has a result in inconsistent change to LNP size which is expected in a polydisperse system .

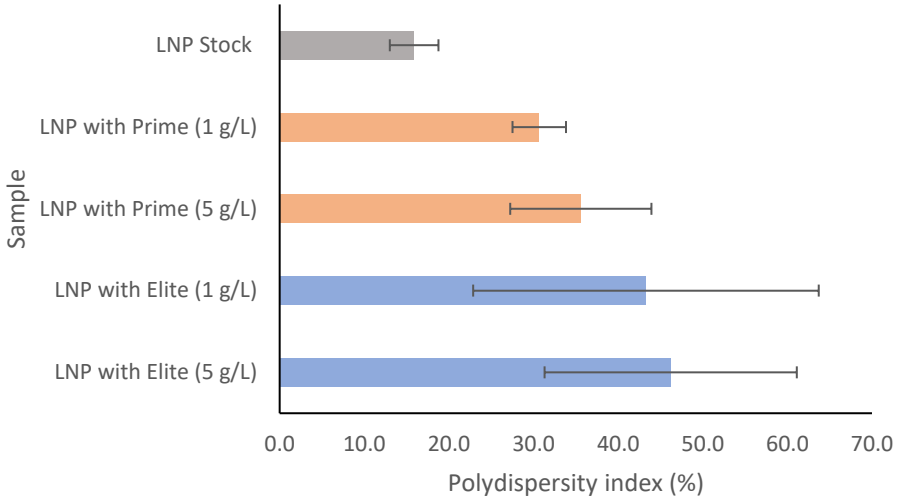


Figure 8: A Bar chart showing the average polydispersity index of LNP on its own and LNP mixed with 1 and 5 g/L of rHA Recombumin® Prime and Recombumin® Elite. The data produced n=3 ±SD (excluding LNP Stock where n=1 ±SD).

Figure 9 shows the ζ-potential of 1:4 LNPs: This concentration was chosen as the LNPs were most stable and at their greatest ζ-potential without the addition of either rHA Recombumin® Prime or Recombumin® Elite at -15.8mV±2.9. The addition of rHA Recombumin® Elite 1 and 5 g/L resulted in reduction in ζ-potential strength, producing -10.3±2.2 mV and -7.6±2.4 mV.

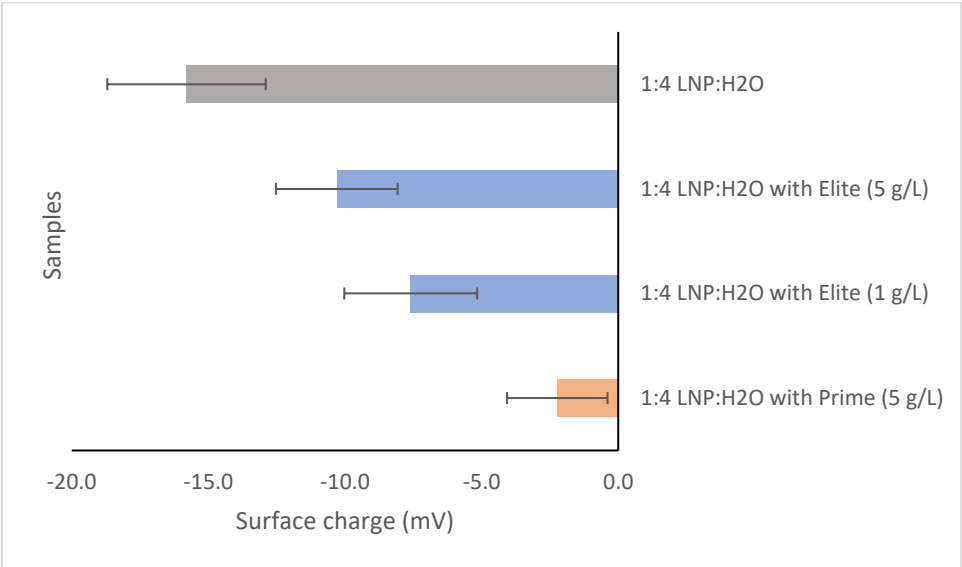


Figure 9: A bar chart showing the Zeta ζ-potential of LNPs in a 1:4 dilution with 0.1µm filtered de-ionised water, mixed with Recombumin® Prime 5 g/L and Recombumin® Elite 5 g/L and 1 g/L. The

results with Recombumin® rHA mixed ±SD where n=3, except 1:4 LNP:H2O where n=1 and ±SD was taken from the cumulant.

Table 4: A Table showing the average radius, polydispersity and zeta ζ-potential of LNP stock and LNP mixed with rHA *Recombumin®* Prime and *Recombumin®* Elite at 5 g/L and 1 g/L. **Note:** zeta ζ-potential was recorded at 1:4 LNP:H2O dilutions for all samples**.**

| Dilution | Radii ±S D | PDI (%) ± SD | Zeta ζ-potential ± SD |
|---|---|---|---|
| 1 g/L Recombumin® Prime | 144.8±7 | 30.7±3.2 | N/A |
| 5 g/L Recombumin® Prime | 152.4±8.5 | 35.6±8.3 | -2.2±1.8 |
| 1 g/L Recombumin® Elite | 174.1±36.6 | 43.3±20.4 | -7.6±2.4 |
| 5 g/L Recombumin® Elite | 166.2±7.1 | 46.2±14.9 | -10.3±2.2 |
| Stock LNP | 131.8±4.2 | 17.8±2.9 | -15.8±2.9 |

However, the addition of rHA Recombumin® Prime produced a ζ-potential of -2.2±1.8 mV, resulting in the greatest loss of surface charge with a 13.6 mV difference between the rHA Recombumin® Prime sample and LNPs without albumin surface charge. A ζ-potential of -2.2 mV suggests the addition of 5 g/L rHA Recombumin® Prime could have destabilised the surface charge of the molecule increasing the chance of intramolecular interactions.

## 4.2. SEC-MALS

### *4.2.1. Waters GTX 2000Å Column using a 10% PBS (pH 7.0) buffer*

Control samples were produced using the most concentrated sample of LNP (367ng), rHA Recombumin® Prime at 1 g/L in 1x PBS (pH 7.0) tested for absorbance at 280nm, usually used for protein identification. After a 50µl injection the green and red curves seen in key of Figure 10 show a main elution peak at 11.7 minutes with a shoulder peak at 11.4 minutes in the mixed sample. This could indicate rHA elution at 11.4 minutes and the later elution the LNP. This would be unexpected due to their size and weight.

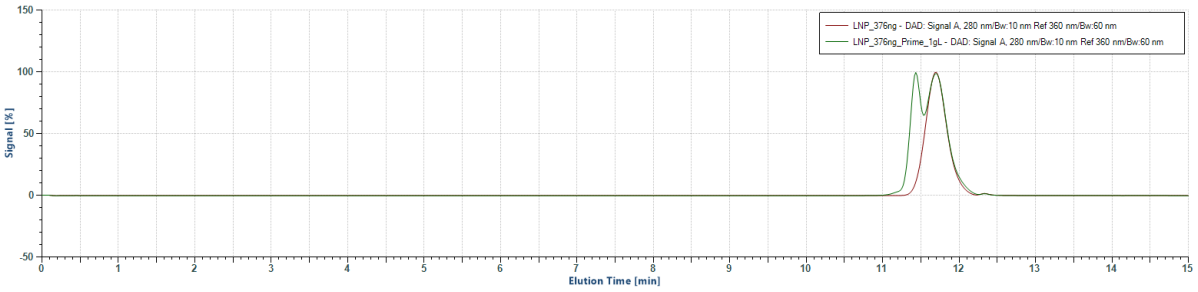


Figure 10: LNP (367ng), and equivalent LNP- rHA (1 g/L) mixture separation with 280 nm UV absorbance individually scaled with Waters GTX 2000Å column and 10% PBS (pH 7.0) elution buffer.

Control standards were produced using the most concentrate sample of LNP (367ng), a diluted sample of LNP in 1x PBS (pH 7.0) (47ng), and rHA Recombumin® Prime at 1 g/L in 1x PBS (pH 7.0) and mixture testing for absorbance at 260nm, commonly used for nucleic acid identification. Figure 11 shows the LNP only samples (367 and 47 ng) elution to be later than the LNP with rHA Recombumin® Prime, the strong peak produced is indicative of the nucleic acid-based cargo within the LNP. The LNP sample elution peaks are similar ranging from 11.7-11.9 minutes. The two peaks being close together the solvent front change indicates there is some resolving power with the column but is limited with

the difference in size between the two tested samples and a possibility of interaction within the column as the LNP is eluting near the solvent front.

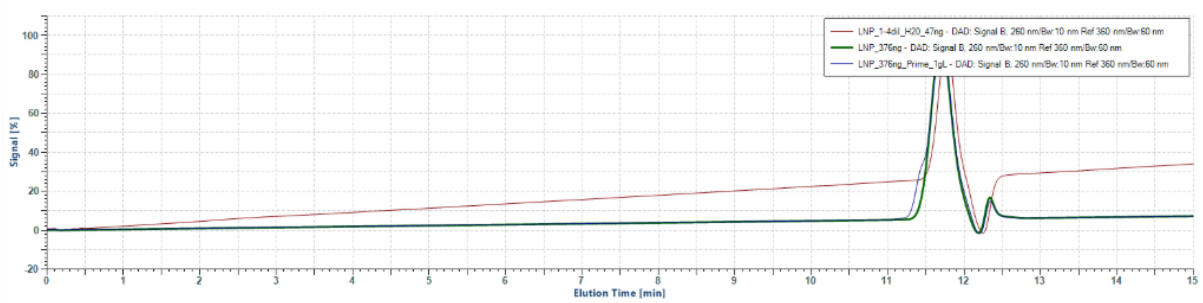


Figure 11: LNP (367ng), rHA (1 g/L) and equivalent LNP- rHA (1 g/L) mixture separation with 260 nm UV absorbance and separation with the Waters GTX 2000Å column and 10% PBS (pH 7.0) elution buffer.

Figures 12 and 13 show the static light scattering (SLS) at 90°. The rHA Recombumin® Prime bound LNPs (blue) elute slightly earlier than the rHA Recombumin® Prime sample (blue). The 376ng LNP sample (red) has a small peaked in Figure 12 when SLS is normalised to the greatest peak in Figure 13, eluting at around 9 mL with remnants suspected to be remainder albumin eluting at around 11 mL. Figure 13, which is normalise individually can be seen with greater signal peak at the 9 mL. To determine whether the ionic strength of the elution buffer affects the potential interaction and 'sticking' of the LNPs to the column the buffer was tested at two increased concentrations, 0.3X and 1XPBS (pH 7.0).

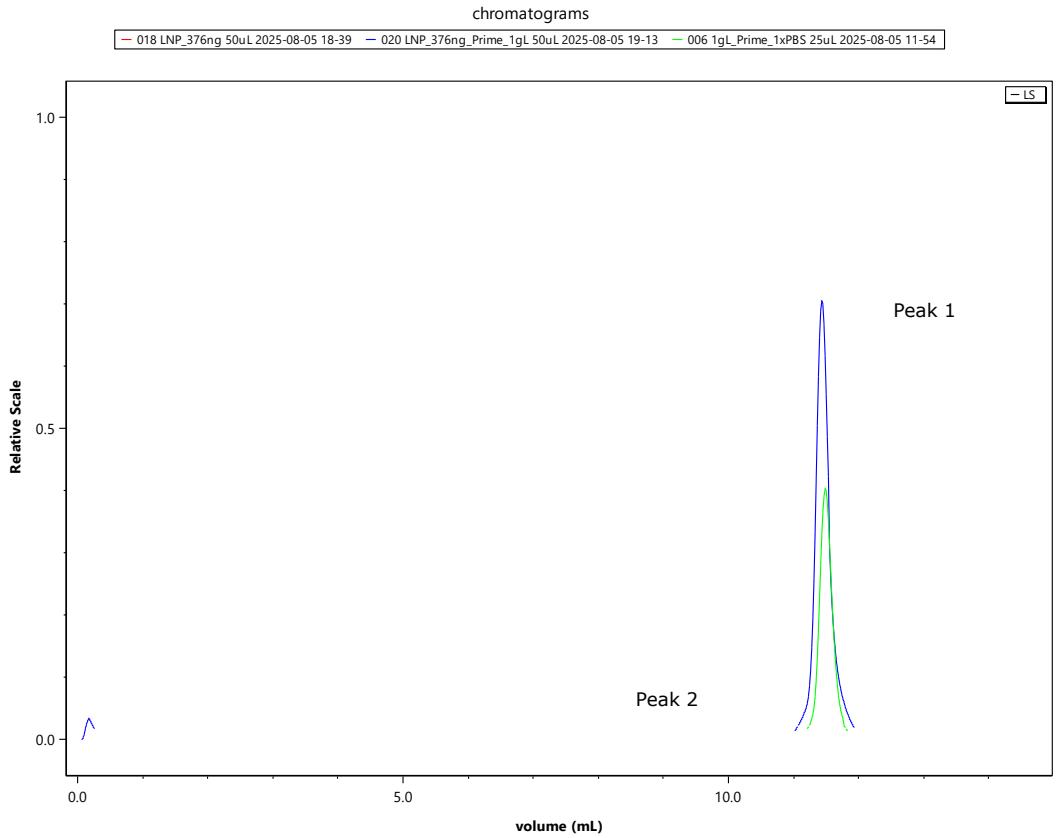


Figure 12: LNP (367ng), rHA (1 g/L) and equivalent LNP- rHA mixture separation light scattering globally scaled with Waters GTX 2000Å column and 10% PBS (pH 7.0) elution buffer.

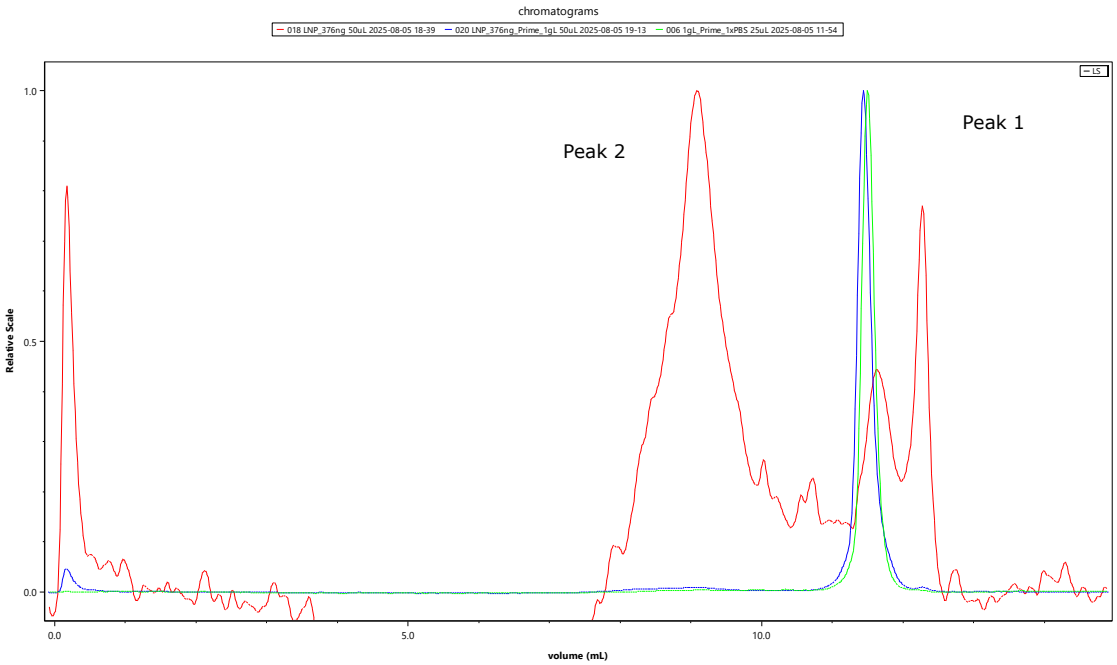


Figure 13: LNP (367ng), rHA (1 g/L) and equivalent LNP- rHA mixture separation light scattering individually scaled with Waters GTX 2000Å column and 10% PBS (pH 7.0) elution buffer.

*4.2.2. 30% PBS (pH 7.0) elution with Waters GTX 2000Å Column*

A 30% PBS (pH 7.0) elution buffer was used with an aim to increase the ionic strength of the elution buffer and prevent LNP from sticking to the column. In addition, the sample size of the LNP used was increased from 50µL to 100µL to increase the LNP concentration from 376ng to 752ng. The concentration of rHA Recombumin® Prime tested was also increased to 5 g/L.

Figure 14 shows the absorbance at 280nm UV of LNP (752ng) and equivalent LNP-rHA (5 g/L). Although a similar profile is shown when compared to Figure 10, the elution time of the LNP has shifted 0.2 minutes later to 11.9 minutes and 11.7 minutes for the rHA Recombumin® Prime. This indicates greater interaction between the LNP, and the column has occurred. 1x PBS (pH 7.0) buffer was trialled to determine if a higher ionic strength of the elution buffer could improve the results produced

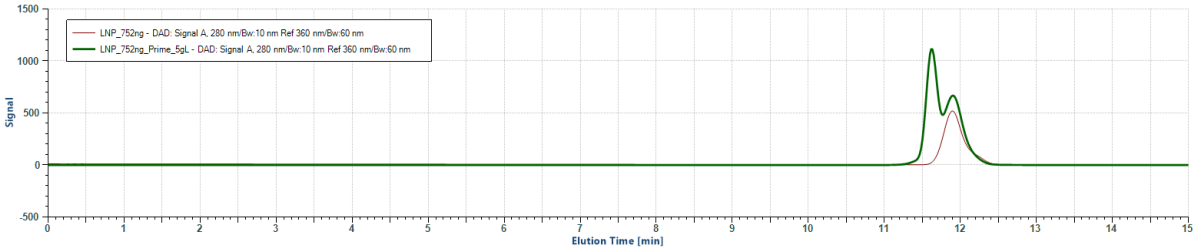


Figure 14: LNP (752ng), and equivalent LNP- rHA (1 g/L) mixture separation with 280 nm UV absorbance and separation with the Waters GTX 2000Å column and 30% PBS (pH 7.0) elution buffer.

*4.2.3. 1x PBS (pH 7.0) Elution with Waters GTX 2000Å Column*

1x PBS (pH 7.0) elution buffer was used to test the same samples tested for the 30% PBS (pH 7.0) elution buffer. The samples were run twice and a control of rHA Recombumin® Prime (5 g/L) was included in this set of testing.

Figure 15 shows the absorbance of the samples described above at 280nm UV. Like Figure 12, the LNP had an elution time of about 11.9 and 11.7 minutes for the albumin. We can ascertain from these results that increasing the ionic concentration of the elution buffer increases the elution time, with the samples most likely interacting with the column to a greater effect as the ionic charge increases.

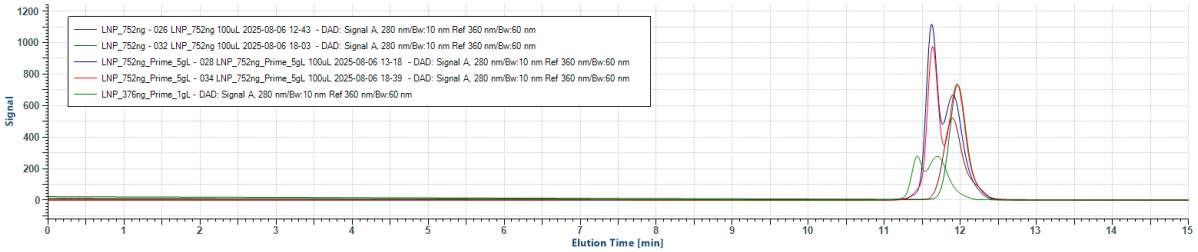


Figure 15: LNP and equivalent LNP- rHA mixture separation comparison of rHA Recombumin® Prime samples and LNP without rHA when tested with 280 nm UV absorbance and separated with the Waters GTX 2000Å column with 100% PBS (pH 7.0) elution buffer.

4.2.4. Molar Mass determination using Waters GTX 1000Å Column with a 0.1XPBS (pH 7.0) buffer

A Waters GTX 1000Å Column using a 0.1XPBS (pH 7.0) buffer was used to see if greater resolution and reduced LNP interaction could be achieved using a column with a small pore size.

Figure 16 shows elution profile of Recombumin® Prime and Recombumin® Elite at 1 g/L and 5g/L as collected through the static light scattering. All four concentrations have a well-defined peak 1 eluting at 10.4 minutes shown in table 5 to have an average Molar Mass (Mw) of 63.8±1.04 kDa (table 5) across all four samples in indicating Peak 1 to be monomer with a monodisperse population with a poly dispersity (Mw/Mn) to be 1 for all samples.

Peak 2, seen in Figure 16, shows rHA samples eluting around 9.8 minutes and PDI of 1. The average Mw of Peak 2 was 149.4±12.8 kDa, twice that of Peak 1 and so was determined to be rHA sample dimer.

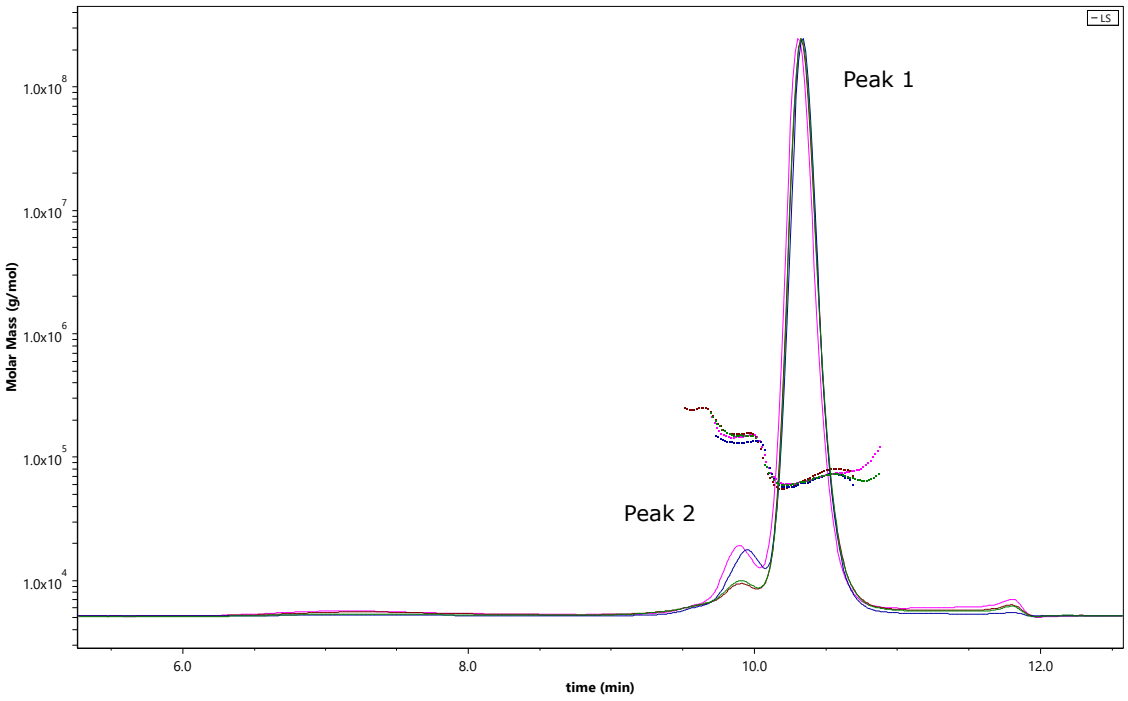


Figure 16: Superimposed Static light scattering signal (Molar Mass vs Time) of Recombumin® Prime and Recombumin® Elite at 1 g/L and 5 g/L, separated with the Waters GTX 1000Å column and 0.1XPBS (pH 7.0) elution buffer

Table 5: Molar Mass (±SD) and polydispersity (±SD) of control samples for rHA Recombumin® Prime and Recombumin® Elite 1 g/L and 5 g/L

| | **Peak 1** | | | | **Peak 2** | | | |
|---|---|---|---|---|---|---|---|---|
| | Mw (kDa) | SD | Polydispersity (Mw/Mn) | SD | Mw (kDa) | SD | Polydispersity (Mw/Mn) | SD |
| **1 g/L_ Recombumin® Prime_1xPBS** | 64.5 | 0.40 | 1 | 0.60 | 148.6 | 0.60 | 1 | 0.80 |
| **5 g/L_ Recombumin® Prime_1xPBS** | 62.3 | 0.40 | 1 | 0.60 | 131.8 | 0.30 | 1 | 0.50 |
| **5 g/L_ Recombumin® Elite_1xPBS** | 63.9 | 0.30 | 1 | 0.40 | 155.4 | 0.30 | 1 | 0.40 |
| **RS10** | 59.7 | 0.30 | 1 | 0.30 | 126.1 | 0.30 | 1 | 0.40 |
| **1 g/L_ Recombumin® Elite_1xPBS** | 64.5 | 0.40 | 1 | 0.60 | 161.6 | 1.00 | 1.1 | 1.40 |

LNP without the addition of any albumin was tested as a baseline to determine the elution profile of LNP on its own. . Figure 17 shows the light scattering (red), $UV_{280nm}$ absorbance (green) and dRI (blue) of the LNP (752ng) sample without the addition of rHA.

As seen in the SLS data (Figure 17), elution of the LNP from the separation column, occurs between 5.7 minutes to 10.9 minutes, fully eluting with the solvent front of the elution buffer, shown by the dRI. $UV_{260nm}$ shows a highly resolute, narrow peak indicating the presence of Poly (A) within peak 1 of the sample, eluting at 10.9 minutes.

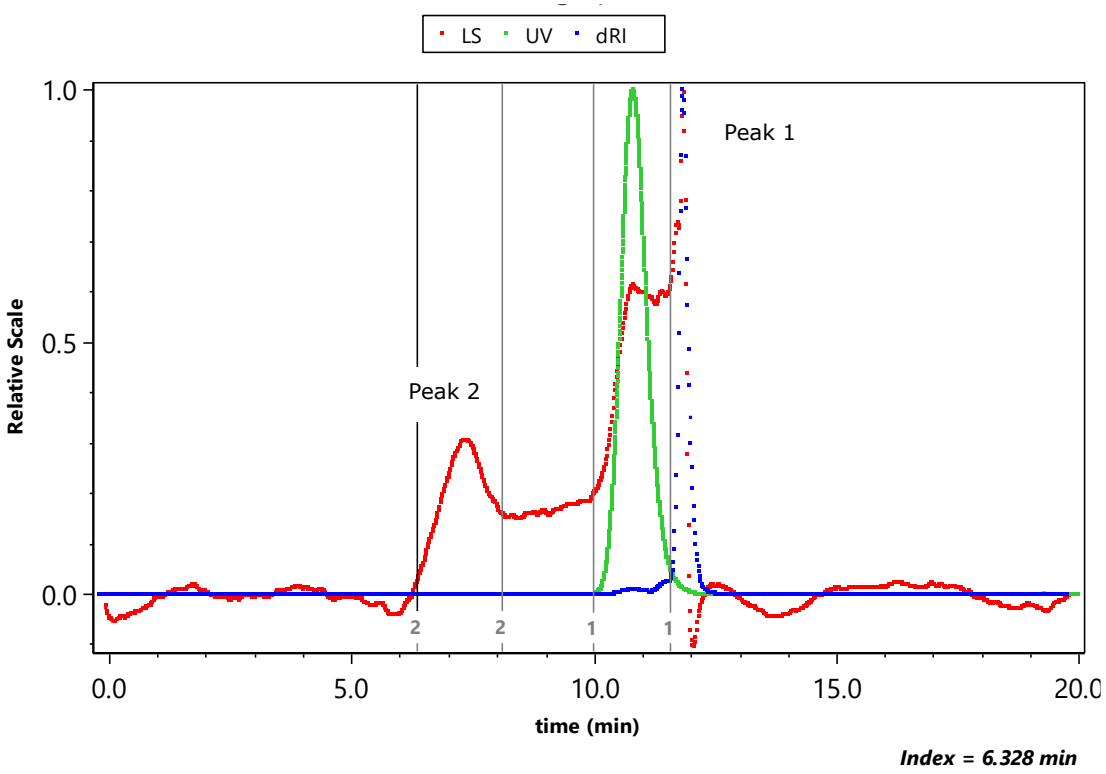


Figure 17: Light scattering (red), UV absorbance at 280nm (green) and dRI (blue) of LNP (752ng), separated with the Waters GTX 1000Å column and 0.1XPBS (pH 7.0) elution buffer.

However, SLS shows Peaks 1 and 2 to have poor resolution (unlike the testing of rHA Recombumin® Prime and Recombumin® Elite) indicating the presence of more than one species with molar mass of 11.1±1.0 kDa and 3398±4.1 kDa respectively. High polydispersity and heterogeneity (Table 6) did not allow to draw definitive conclusion

.

Figure 18 shows how the addition of 1 g/L rHA Recombumin® Prime affected the elution profile of LNPs. The figure shows the static light scattering (red), UV absorbance at 280 nm (green) and dRI (blue).

A broad, shouldered peak can be seen in Figure 18, signifying the presence of Poly (A) (Peak 1) and rHA Recombumin® Prime (Peak 2), further shown by the elution times of 10.8 (Figure 16) and 10.4 (Figure 17) minutes respectively. The molar mass of peaks 1 and 2 (Figure 18) are similar to the molar mass of rHA monomer and dimer structures seen in Peaks 1 (~60 kDa) and 2 (~120 kDa) (Table 6).

Figure 18 Peak 3 (Mw – 401.3±1.3 kDa) and 4 (Mw - 4436.5±2.5) were speculated to be rHA trimer and LNP peaks respectively. However, both peaks had a greater molar mass than would be expected of the rHA timer (Mw ~ 180 kDa) or LNP (Mw - 3398±4.1 kDa, Table 6, LNP 752ng Peak 3), further experimentation and refinement of testing parameters is necessary for more conclusive analysis.

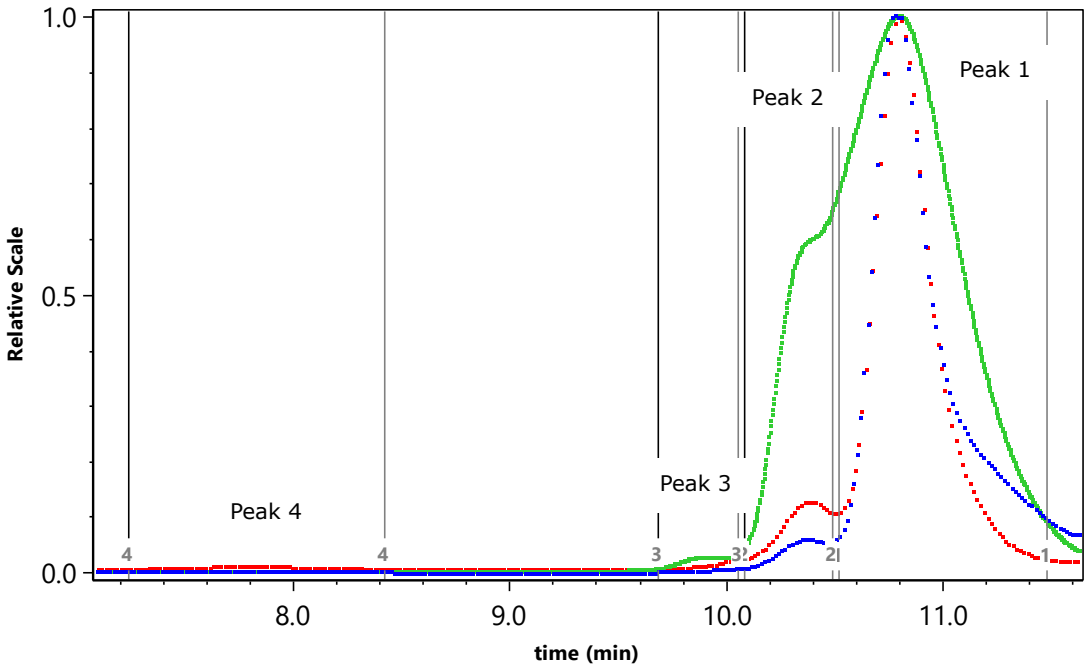


Figure 18: SLS (red), UV absorbance at 280 nm, and dRI of LNP (752) mixed with rHA Recombumin® Prime at 1 g/L, separated with the Waters GTX 1000Å column and 0.1XPBS (pH 7.0) elution buffer.

Table 6: Molar Mass (Mw) ±SD and polydispersity (PDI) ±SD of LNP (752 ng) without rHA and with rHA Recombumin® Prime and Recombumin® Elite at 1 g/L and 5 g/L.

| | **Peak 1** | | **Peak 2** | | **Peak 3** | | **Peak 4** | |
|---|---|---|---|---|---|---|---|---|
| | Mw (kDa) ±SD | PDI (Mw/Mn) ±SD | Mw (kDa) ±SD | PDI (Mw/Mn) ±SD | Mw (kDa) ±SD | PDI (Mw/Mn) ±SD | Mw (kDa) ±SD | PDI (Mw/Mn) ±SD |
| **LNP_752ng** | 11.1 ± 1.0 | 1.4± 1.5 | 3398± 4.1 | 2.9 ± 13.8 | - | - | - | - |
| **LNP_752ng_5g/L Recombumin® Prime** | 59.5 ± 0.3 | 1± 0.4 | 132.4±0.2 | 1±0.3 | - | - | - | - |
| **LNP_752ng_1g/L Recombumin® Prime** | 55.7±0.4 | 1.1±0.7 | 140.1± 0.3 | 1±0.4 | 401.3 ± 1.3 | 1.2± 1.7 | 4436.5± 2.5 | 1.2±3.8 |
| **LNP_752ng_ Recombumin® Elite_5 g/L** | 61.2± 0.3 | 1 ± 0.4 | 155.7 ± 0.3 | 1 ± 0.4 | 10153 ± 1.3 | 1.2 ± 1.8 | - | - |
| **LNP_752ng_ Recombumin® Elite_1 g/L** | 58.5±0.3 | 1.1 ±0.5 | 170.2 ±0.3 | 1.1 ±0.4 | - | - | - | - |

# 5. Discussion

With an aim to identify the successful LNP production in the suitable conditions such changes in the salt concentrations, surface charge and particle size distribution of LNPs were tested in the presence and absence of albumin.

The LNPs were diluted in 1XPBS (pH 7.0) and tested in a dilution series, from 1:2 to 1:40, to identify the limits of detection for both methods regarding concentration of LNP and buffer salt concentration.

Measuring the hydrodynamic radius of LNPs diluted in 1XPBS (pH 7.0) using DLS (Figure 3), a decrease in radius can be seen across the dilution range, with the average radius being 124.5±9.4 nm. We found the 1XPBS (7.0) to be unsuitable for ζ-potential measurements due to the production of bubbles. When placed in an electrophoretic environment, the high salt content of 1XPBS (7.0) causes electrolysis of the sample, damaging the LNP and preventing laser detection of the sample. Three other diluents 0.1PBS, 0.5XPBS and water were tested for their suitability for ζ-potential experiments, water was used to view the sample with no addition of salt. The surface charge of LNPs in these conditions and their hydrodynamic radius were measured to determine the most suitable diluent. LNPs diluted in 0.1XPBS (7.0) were found to have the most consistent size and surface charge across the dilution's series (Figures 3 and 4), it had an average radius of 128.0±6.2 nm and average charge of 19.9±5.5 mV. Although 0.1XPBS was the most suitable for testing the ζ-potential of LNPs by themselves, water was used when LNPs were tested with different Recombumin® rHA formulations. This is because of the presence of high concentration of salts in Recombumin® rHA formulations. With a greater timeframe for the experiment more buffer

concentrations would be tested for consistent size and charge to be produced for LNPs with and without rHA.

Albumin is a 66.5kDa large protein forming 50% of all proteins found in the blood serum with a half-life of approximately 19 days. Albumin has multiple therapeutic and pharmaceutical applications (Elsadek and Kratz, 2012).

For example, the addition of albumin can form a corona on the surface of nanoparticles extending the therapeutic half-lives of nanoparticles and enhancing their ability for deterrence of immunological responses and increasing cellular up-take via endosomes (Lacroix, Fakih and Sleiman, 2020). We aimed to determine the suitable characterisation method to determine successful LNP production and its solution properties in different salt concentrations. Addition of albumin to the LNP provided another insight into the changes in hydrodynamic characteristics in the presence of another moiety.

Testing of LNPs mixed with rHA Recombumin® Prime and Recombumin® Elite 1 g/L and 5 g/L (Figure 7) with DLS was used to identify an increase in hydrodynamic radius. The increased %intensity and average radius of Peak 2, seen in Figure 6, signifies a potential Recombumin® rHA interaction to LNP molecules, however, the nature of the interaction requires further testing for greater insight. The average radii of LNP samples with rHA to have increased when compared to the average radii of LNP without rHA (131.8±4.2 nm). Figure 7 shows the addition of rHA Recombumin® Elite to cause the greatest increase in LNP radii, with a 43 nm increase in radius between initial LNP testing and LNPs with 1 g/L rHA Recombumin® Elite (174.1±36.6 nm). This could be due to flocculation as suggested by larger standard deviation. Alternatively, there is a slight possibility that 1 g/L Recombumin® Elite has a greater binding affinity in comparison to the

other samples which could possibly have resulted in formation of thicker surface corona. Nevertheless, this requires further investigation.

The ζ-potential recorded for all LNP samples in the presence of rHA had a smaller surface charge than LNPs without the addition of rHA. This may be a result of the salt concentration present in the initial rHA Recombumin® Prime and Recombumin® Elite formulations. Excess salt within the sample, as seen with 1XPBS, can induce electrolysis as well as dehydration of LNPs as surface hydrate is in competition, reducing the surface charge of the molecule, increasing the change of flocculation and aggregation (Francis et al., 2025). A larger time frame for the experiment would allow for testing of LNPs across a range of dilutions and rHA concentrations to find the most suitable parameters for testing LNPs in the presence of Recombumin.

SEC-MALS is an absolute characterisation technique capable of separating species by molecular weight and size through high pressure liquid chromatography (HPLC) and determining concentration and radius through different light scattering and absorbance techniques. We used SEC-MALS to confirm data produced during DLS about LNP and albumin interaction and the characteristics of the subsequent compound. Two columns with different pore sizes were tested to evaluate better separation of components.

With 2000A° column, Initial absorbance testing at 280nm UV of (relatively) undiluted LNP (376 ng)-rHA Recombumin® Prime (1 g/L) produced a dual peak curve. These peaks formed at 11.4 minutes elution and 11.7 minutes elution, the latter shown as the LNP (376 ng) when comparing the two samples. DLS has shown rHA Recombumin® Prime to be 4.1 nm in diameter and undiluted LNP to be ~130nm, further increasing in size when in complex with rHA Recombumin® Prime.

LNP would be expected to elute prior to free, unbound albumin in the sample mixture. Instead LNPs can be seen in Figure 10 eluting after the albumin near the solvent front suggesting interaction to the column. In addition, testing 1 g/L rHA Recombumin® Prime with SLS at 90° (Figure 12) shows a clear albumin peak (Peak 1, green), at around 11.5 mL. In contrast LNP (376 ng) has a very small peak (peak 2) eluting around 9mL, this peak is shown clearer in Figure 13. SLS signal intensity produced during LNP (376 ng) testing is surrounded by lots of background noise as a result of a small concentration signifying possible LNP interaction with the column.

In order to determine whether LNP elution time could be reduced to give better resolution between Recombumin® rHA and LNP, two other salt concentrations of the elution buffer were tested to see if an improvement on LNP elution could be made. In total 0.1X, 0.3X and 1XPBS (pH 7.0) were trailed. Comparing the UV absorbance at 280 nm of the three buffers in Figure 15 the 0.1XPBS (green) performed the best eluting the earliest at 11.7 minutes, while 0.3XPBS and 1XPBS (blue and orange) eluted roughly 12 seconds later at 11.9 minutes. This shows increasing the salt concentration by a large amount does not reduce the elution time. Future identification of solutions includes testing other parameters such as pore size, flow rate or use polymer-based column.

SEC-MALS was repeated using a Waters GTX 1000Å separation column with 0.1XPBS (pH 7.0) elution buffer. Initial testing of Recombumin® Prime and Recombumin® Elite at 1 g/L and 5 g/L presented defined peaks with clear resolution of two species, an rHA monomer and dimer for all samples (Figure 16). On average, Peak 1 eluted at 10.4 minutes, while Peak 2 eluted at 9.8 minutes, in addition to a PDI of 1 for all samples, the rHA Recombumin® Prime and

Recombumin® Elite 1 g/L and 5 g/L control samples produced reliable results for future comparison. On the other hand, LNP (752 ng) without the addition of rHA (Figure 17), presents two; broad and unresolved peaks, ranging in elution time from 5.7 to 10.9 minutes. subsequent UV absorbance at 260 nm showed Poly (A) to elute at Peak 2 (10.7 minutes) signifying a possibility of two species present between peaks 1 and 2.

The molar mass of LNP Peak 1 was 11.1±1.0 kDa and that of peak 2 was 3398±4.1 kDa (Figure 17) with a PDI of 1.4±1.5 and 2.9±13.8, respective to Peak 1 and Peak 2 (table 6). As a result of broad peaks, high polydispersity and poor separation resolution, no conclusive definitions of the two peaks can be drawn. The potential for a second species may suggest issues in the formulation methodology or be a result of degradation during storage (4$^{o}$C). However, further testing is required to find parameters suitable in order to produce clear and reproducible data.

During this study we used silica-based columns (2000Å and 1000Å) Silica a polar molecule which has a possibility of non-covalant interaction, as seen with the Waters GTX 2000Å column. Polymer based column on the other hand can have reduced intermolecular interactions. However, polymer-based columns often have reduced resolution, with larger pore sizes in comparison to silica-based columns (Lee et al., 2025). Nevertheless, it will be worth testing the difference in LNP elution profile of non-silica-based columns.

Further identification of key parameters such as concentration, temperature, which affect LNP physiochemical composition may reduce the fluidity of the complex, reducing the chances of column or intramolecular interactions (Lee et al., 2025).

# 6. Conclusion

Successful formulation of LNPs using herringbone microchip method allowed for the development of biophysical testing methods for size and charge using DLS and ζ-potential. It was found using the method described, LNPs dialysed 1XPBS (pH 7.0) produced LNPs with an average radius of 124.5±9.4 nm and when diluted in 0.1XPBS (pH 7.0) produced an average ζ-potential of -16.1±4.4 mV. The addition of Recombumin® rHA to resulted biophysical changes to the LNP, increasing in radii, indicating ligation to the lipid complex. However, surface charged decreased when compared to LNPs tested without rHA. If time had allowed a RiboGreen assay to determine encapsulation efficiency of LNP would have been carried out and whether presence of albumin with LNP would affect the assay outcomes.

SEC-MALS required further testing of parameters. Using a Waters GTX 2000Å column had too little resolution and interactions with the column resulted in the LNPs eluting after unbound albumin, and too little concentration for definitive identification of LNP. It was found, however, the use of 0.1XPBS (pH 7.0) resulted in an elution profile with the best resolution when compared to 0.3X and 0.5XPBS (pH7.0).

Using the Waters GTX 1000Å column, with a 0.1XPBS (pH7.0) elution buffer, we were able to successfully determine the molecular weights of rHA Recombumin® Prime and Recombumin® Elite at 1 and 5 g/L. Measurement of LNP requires further refinement due to broad peaks and subsequent polydispersity produced during SLS data collection. Further experiments explore may differing temperatures, reduced column pore sizes, differing column material and makes in order to determine suitable parameters for clear and repeatable data collection.

# 7. References


**[1]** Baños, C.-E., Wiedmer, S.K., Smått, J.-H., Sakeye, M., Lokajová, J. and Riekkola, M.-L. (2012). Phospholipids covalently attached to silica particles as stationary phase in nano-liquid chromatography. *Journal of Pharmaceutical and Biomedical Analysis*, [online] 71, pp.1–10. doi:https://doi.org/10.1016/j.jpba.2012.08.006.

**[2]** Caraceni, P., Tufoni, M. and Bonavita, M.E. (2013). Clinical Use of Albumin. *Blood Transfusion*, [online] 11(Suppl 4), pp.s18–s25. doi:https://doi.org/10.2450/2013.005s.

**[3]** Chauhan, I., Yasir, M., Verma, M. and Singh, A.P. (2020). Nanostructured Lipid Carriers: a Groundbreaking Approach for Transdermal Drug Delivery. *Advanced Pharmaceutical Bulletin*, [online] 10(2), pp.150–165. doi:https://doi.org/10.34172/apb.2020.021.

**[4]** Elsadek, B. and Kratz, F. (2012). Impact of Albumin on Drug Delivery — New Applications on the Horizon. *Journal of Controlled Release*, 157(1), pp.4–28. doi:https://doi.org/10.1016/j.jconrel.2011.09.069.

**[5]** Francis, J.A., Wright, L., van Wegen, R., Zhao, C.-X. and Falconer, R.J. (2025). Effects of salts, buffers and sucrose on protein–protein attractive and repulsive interactions. *International Journal of Pharmaceutics*, 672, p.125321. doi:https://doi.org/10.1016/j.ijpharm.2025.125321.

**[6]** Haque, Md.A., Shrestha, A., Mikelis, C.M. and Mattheolabakis, G. (2024). Comprehensive analysis of lipid nanoparticle formulation and preparation for RNA delivery. *International Journal of*

*Pharmaceutics: X*, [online] 8, p.100283. doi:https://doi.org/10.1016/j.ijpx.2024.100283.

**[7]** Johnson, L.T., Zhang, D., Zhou, K., Lee, S.M., Liu, S., Dilliard, S.A., Farbiak, L., Chatterjee, S., Lin, Y.-H. and Siegwart, D.J. (2022). Lipid Nanoparticle (LNP) Chemistry Can Endow Unique *In Vivo* RNA Delivery Fates within the Liver That Alter Therapeutic Outcomes in a Cancer Model. *Molecular Pharmaceutics*, 19(11), pp.3973–3986. doi:https://doi.org/10.1021/acs.molpharmaceut.2c00442.

**[8]** Jung, H.N., Lee, S.-Y., Lee, S., Youn, H. and Im, H.-J. (2022). Lipid nanoparticles for delivery of RNA therapeutics: Current status and the role of *in vivo* imaging. *Theranostics*, 12(17), pp.7509–7531. doi:https://doi.org/10.7150/thno.77259.

**[9]** Jürgens, D.C., Deßloch, L., Porras-Gonzalez, D., Winkeljann, J., Zielinski, S., Munschauer, M., Hörner, A.L., Burgstaller, G., Winkeljann, B. and Merkel, O.M. (2023). Lab-scale siRNA and mRNA LNP Manufacturing by Various Microfluidic Mixing Techniques – an Evaluation of Particle Properties and Efficiency. *OpenNano*, [online] 12, p.100161. doi:https://doi.org/10.1016/j.onano.2023.100161.

**[10]** Lacroix, A., Fakih, H.H. and Sleiman, H.F. (2020). Detailed cellular assessment of albumin-bound oligonucleotides: Increased stability and lower non-specific cell uptake. *Journal of Controlled Release*, [online] 324, pp.34–46. doi:https://doi.org/10.1016/j.jconrel.2020.04.020.

**[11]** Lee, J., Yoshimoto, N., Takase, H., Watanabe, N.M., Okamoto, Y. and Hiroshi Umakoshi (2025). Interaction Analysis between Cationic Lipid and Oligonucleotide with a Lipid Membrane-Immobilized Monolith Silica Column: A High-Performance Liquid Chromatography Approach. *Langmuir*. doi:https://doi.org/10.1021/acs.langmuir.4c03667.

**[12]** Mehta, M., Bui, T.A., Yang, X., Aksoy, Y.A., Goldys, E.M. and Deng, W. (2023). Lipid-Based Nanoparticles for Drug/Gene Delivery: an Overview of the Production Techniques and Difficulties Encountered in Their Industrial Development. *ACS Materials Science Au*, 3(6). doi:https://doi.org/10.1021/acsmaterialsau.3c00032.

**[13]** Nail Minigulov, Kuandyk Boranbayev, Ayaulym Bekbossynova, Bakhytgul Gadilgereyeva and Olena Filchakova (2024a). Structural proteins of human coronaviruses: what makes them different? *Frontiers in Cellular and Infection Microbiology*, 14. doi:https://doi.org/10.3389/fcimb.2024.1458383.

**[14]** Nail Minigulov, Kuandyk Boranbayev, Ayaulym Bekbossynova, Bakhytgul Gadilgereyeva and Olena Filchakova (2024b). Structural proteins of human coronaviruses: what makes them different? *Frontiers in Cellular and Infection Microbiology*, 14. doi:https://doi.org/10.3389/fcimb.2024.1458383.

**[15]** Suk, J.S., Xu, Q., Kim, N., Hanes, J. and Ensign, L.M. (2016). PEGylation as a Strategy for Improving nanoparticle-based Drug and Gene Delivery. *Advanced Drug Delivery Reviews*, [online] 99, pp.28–51. doi:https://doi.org/10.1016/j.addr.2015.09.012.

**[16]** Wang, J., Ding, Y., Chong, K., Cui, M., Cao, Z., Tang, C., Tian, Z., Hu, Y., Zhao, Y. and Jiang, S. (2024). Recent Advances in Lipid Nanoparticles and Their Safety Concerns for mRNA Delivery. *Vaccines*, [online] 12(10), p.1148. doi:https://doi.org/10.3390/vaccines12101148.